

~~Toward~~ Towards a coupled model to investigate wave-sea ice interactions in the Arctic marginal ice zone

Guillaume Boutin¹, Camille Lique¹, Fabrice Ardhuin¹, Clément Rousset², Claude Talandier¹, Mickael Accensi¹, and Fanny Girard-Ardhuin¹

¹Univ. Brest, CNRS, IRD, Ifremer, Laboratoire d'Océanographie Physique et Spatiale, IUEM, Brest, France

²Sorbonne Universités (UPMC Paris 6), LOCEAN-IPSL, CNRS/IRD/MNHN, Paris, France

Correspondence: boutinguillaume87@gmail.com

Abstract. The Arctic Marginal Ice Zone (MIZ), where strong interactions between sea ice, ocean and atmosphere are taking place, is expanding as the result of ~~the~~ on-going sea ice retreat. Yet, ~~state-of-art models are not capturing the complexity of the varied processes occurring in the MIZ, and in particular the processes involved in the~~ state-of-the-art models exhibit significant biases in their representation of the complex ocean-sea ice interactions. ~~In the present study, a coupled sea ice-wave model is developed, in order to improve our understanding and model representation of those interactions. The coupling allows us~~ taking place in the MIZ. Here, we present the development of a new coupled sea ice-ocean wave model. This set up allows us to investigate some of the key processes at play in the MIZ. In particular, our coupling enables to account for the wave radiative stress resulting from the wave attenuation by sea ice, and the sea ice lateral melt resulting from the wave-induced sea ice ~~break-up. We found fragmentation. We find~~ that, locally in the MIZ, the ocean surface waves can affect the sea ice drift and melt, resulting in significant changes in sea ice concentration and thickness as well as sea surface temperature and salinity. Our results highlight the need to include ~~the~~ wave-sea ice processes in models ~~aiming at forecasting used to forecast~~ sea ice conditions on short time ~~scale, although scales. Our results also suggest that~~ the coupling between waves and sea ice would ~~probably required ultimately need~~ to be investigated in a more complex system, allowing for interactions with the ocean and the atmosphere.

1 Introduction

Numerical models exhibit large biases in their representation of ~~the~~ Arctic sea ice concentration and thickness, regardless of their complexity or resolution (Stroeve et al., 2014; Chevallier et al., 2017; Wang et al., 2016; Lique et al., 2016). Comparing 10 reanalyses based on state-of-the-art ocean-sea ice models against observations, Uotila et al. (2018) found that ~~the model biases are~~ model biases were the largest in the Marginal Ice Zone (MIZ). Indeed, the MIZ is characterized by a wide variety of processes resulting from the highly ~~non-linear non-linear~~ interactions between the atmosphere, ~~the ocean and the sea ice~~ (Lee et al., 2012), ocean and sea ice: sea ice floe fragmentation and welding, lead opening and associated heat transfers, mesoscale and submesoscale features arising from strong temperature and salinity gradients (see Lee et al., 2012, for a review and references), and many of these processes are only crudely (if at all) taken into account in models. Some of these processes ~~result from the~~

~~interactions between surface wave~~, sea ice fragmentation in particular, result from interactions between ocean surface waves and sea ice, and are thought to be key for the dynamics and evolution of the MIZ (Thomson et al., 2018). These interactions are the focus of the current paper.

~~Summer sea~~

- 5 Sea ice in the Arctic has been drastically receding over the past few decades (Comiso et al., 2017), resulting in an expansion of the MIZ in summer (Strong and Rigor, 2013) which is expected to ~~be intensified~~ intensify in the future (Ak-senov et al., 2017). This ~~offers~~ provides an expanding fetch for waves to grow and propagate (~~Thomson and Rogers, 2014~~) (Thomson and Rogers, 2014; Waseda et al., 2018), suggesting an overall increase of wave heights in the Arctic (~~Stopa et al., 2016b~~) (Stopa et al., 2016a). Once generated, waves can then propagate into sea ice, ~~impacting strongly the dynamical and thermodynamic~~
- 10 strongly impacting both dynamical and thermodynamical sea ice properties in the MIZ through different mechanisms (Asplin et al., 2012). First, observations suggest that waves determine the shape and size of the sea ice floes in the MIZ, through the ~~break-up fragmentation~~ occurring when the ice cover is deformed (Langhorne et al., 1998), or by controlling the formation of frazil/pancake ice (Shen and Ackley, 1991). Wave-induced sea ice fragmentation is also expected to affect lateral melt (Steele et al., 1992), heat fluxes between ocean and atmosphere (Marcq and Weiss, 2012), ~~or~~ and sea ice drift in the MIZ (McPhee,
- 15 1980; Feltham, 2005; Williams et al., 2017). When breaking in the MIZ, waves can generate turbulence in the mixed layer (Sutherland and Melville, 2013), possibly affecting the rate of ice formation or melting by modulating heat fluxes between the ocean, the sea ice and the atmosphere. Observations conducted during a storm in October 2015 in the Beaufort Sea have ~~for instance~~ for instance, revealed that storm-induced waves can lead to an increase of surface mixing and an associated heat entrainment from the upper ocean, resulting in ~~an important large~~ melt of pancake ice (Smith et al., 2018). Finally, waves
- 20 transport momentum, ~~so that and therefore~~ when they are attenuated in the MIZ through reflection or dissipation, part of ~~the~~ their momentum goes into sea ice. This process, called ~~the~~ wave radiative stress (WRS; Longuet-Higgins and Stewart, 1962; Longuet-Higgins, 1977), acts as a force that pushes the sea ice in the direction of ~~the~~ propagation of the attenuated waves. This force is a dominant term in the ice momentum balance ~~on the outskirts of the Southern ocean sea ice in the Southern Ocean~~ MIZ (Stopa et al., 2018b) and it may become more prominent in the Arctic in the future. In return, sea ice strongly attenuates
- 25 waves propagating in the MIZ, either by dissipative processes (e.g. under-ice friction, inelastic flexure, floe-floe collisions) or conservative processes (e.g. scattering) (Squire, 2018).

- Most of the recent efforts in the ~~modeling~~ modelling community have been ~~focusing~~ focused on the impact of sea ice on waves (Dumont et al., 2011; Williams et al., 2013; Montiel et al., 2016), leading to the development of wave models account-
- 30 ing for the presence of sea ice (~~Dumont et al., 2011; Williams et al., 2013; Montiel et al., 2016; Boutin et al., 2018~~) (Boutin et al., 2018). By prescribing sea ice conditions, these models are able to ~~reproduce accurately~~ accurately reproduce the time and space variations of wave height heights in sea ice retrieved from recent field observations (Kohout et al., 2014; Thomson et al., 2018; Cheng et al., 2017) and innovative processing of Synthetic Aperture Radar (SAR) satellite observations (Ardhuin et al., 2017). The good agreement with the observations also suggests a proper representation and quantification of ~~the~~ wave attenuation and propagation in sea ice in these models (Ardhuin et al., 2016; Rogers et al., 2016; Ardhuin et al., 2018). Yet, in this case, sea ice

conditions are only a forcing and thus not affected by waves. This means that these models cannot realistically represent the fate of the sea ice floes once broken by waves, as they do not account for advection, melting and refreezing processes. A first step ~~toward~~ towards the representation of ~~the~~ wave-sea ice interactions was ~~done~~ made by Williams et al. (2013) and Boutin et al. (2018), who included in their respective ~~model~~ models a Floe Size Distribution (~~hereafter~~ FSD) that evolves depending on the sea state. ~~Yet~~ However, considering only ~~the~~ sea ice fragmentation is not sufficient to represent the full complexity of ~~the~~ wave-sea ice interactions.

In ~~contrast, little progress has been done~~ parallel, progress has also been made regarding the inclusion of the effects of waves in coupled ocean-sea ice models. Using a very simple parameterization, Steele et al. (1989) and Perrie and Hu (1997) have investigated the effect of WRS on ~~the~~ sea ice drift in the MIZ, only considering the attenuation of waves generated between the ice floes. ~~They, and~~ found a limited impact on the sea ice conditions. More recently, Williams et al. (2017) ~~have~~ implemented a wave module in the ~~semi-lagrangian~~ semi-Lagrangian sea ice model neXtSIM (Rampal et al., 2016) and found that high ~~waves conditions can induce~~ wave conditions can cause a significant displacement of the sea ice edge. The implementation of FSDs in different sea ice models ~~as done by Zhang et al. (2015) or Horvat and Tziperman (2015) has also allowed the~~ , as introduced by Zhang et al. (2015) and Horvat and Tziperman (2015) for instance, has also opened the way to the assessment of the potential enhancement of lateral melt by wave-induced ice fragmentation (~~Zhang et al., 2016; Bennetts et al., 2017~~) (Zhang et al., 2016; Bennetts et al., 2017; Roach et al., 2018; Bateson et al., 2019), but the representation of waves remains too ~~crude~~ simple to simulate the full effect of waves on the evolution of sea ice.

In the present study, we go beyond ~~the simple inclusion of the forcing of wave~~ simply forcing a wave model by sea ice ~~or of sea ice by wave in models~~ properties, or conversely forcing a sea ice model by wave properties, by proposing a full coupling between a spectral wave model and a ~~state-of-art~~ state-of-the-art sea ice model. The coupled framework allows us to investigate the interactions between waves and sea ice in the Arctic, and the impact that including these effects in a model has on the representation of the ~~wave~~ waves, ocean, and sea ice properties in the Arctic MIZ. We focus in particular on two aspects of these interactions: firstly the effect of including the WRS, computed by the wave model, in the sea ice model, and secondly the wave-induced sea ice fragmentation and its effects on lateral melt through the addition of a FSD in the sea ice model. The remainder of this paper is organized as follows. The different models and configurations used in this study are described in Section 2. Section 3 is devoted to the theoretical and practical implementation of the coupling between the two models. In section 4, we compare ~~pan-Arctic simulations in two~~ pan-Arctic simulations: one for which the coupling between wave and sea ice is implemented ~~or not, in order,~~ and one with the ocean-sea ice model run as stand-alone. Our objective is to quantify the dynamical and thermodynamical impacts ~~on~~ of the coupling on the sea ice and ocean surface properties. A summary and conclusions are given in Section 5.

2 Methods

In this study we make use of the spectral wave model WAVEWATCH III[®] (hereafter WW3; The WAVEWATCH III[®] Development Group, 2016), building on the previous developments ~~performed~~ by Boutin et al. (2018) who included a FSD in WW3 as well as a representation of the different processes by which sea ice can affect the propagation and ~~modulation-attenuation~~ of waves in the MIZ. These processes are scattering (which redistributes the wave energy without dissipation), friction under sea ice (with a viscous and a turbulent part depending on the wave Reynolds number), and inelastic flexion. All these processes depend on sea ice thickness and concentration, and scattering and inelastic flexion also depend on floe size.

We also use the sea ice model LIM3 (Vancoppenolle et al., 2009; Rousset et al., 2015), in which a FSD is first implemented as described in Section 3.2. The model includes a standard Elasto-Visco-Plastic rheology (Hunke and Dukowicz, 1997), using the stress tensor formulation of Bouillon et al. (2013) adapted for the C-grid used in the model. The ice strength is determined following Hibler III (1979), with the ice strength P following $P = P^* h e^{C(1-c)}$, where $P^*=20,000$ N/m² and $C=20$ are empirical positive parameters, and h is the cell-average sea ice thickness. The plastic failure threshold lies on an elliptical yield curve, with the eccentricity set to 2. The number of sub-time steps used to solve the momentum equation is set to 120. The two models are coupled through the coupler OASIS-MCT (Craig et al., 2017). Two configurations of different complexities are used in the following and briefly described in the ~~remaining-remainder~~ of this section.

2.1 Idealized configuration

In order to test and illustrate the effect of the coupling (Section 3), we make use of a simple idealized configuration (see Fig. 1), in which LIM3 is used in a ~~stand-alone-stand-alone~~ mode (without any ocean component). The configuration is a squared domain with 100×100 grid ~~cell~~cells, with a resolution of 0.03° in both directions (corresponding roughly to 3 km). Both models are run on the same grid ~~, and~~ with the same time step set to 300s. The coupling time step is also set to 300steo. The sea ice is ~~only forced~~forced solely by waves, without prescribing any wind or ocean ~~current~~currents. Following Boutin et al. (2018), the simulation starts at rest, with distributions of sea ice concentration (Fig. 1a) and thickness (Fig. 1c) set to represent roughly the conditions that can be found in the MIZ. Starting from the western border, the domain is free of ice over the first $\simeq 10$ km, after which the ice concentration c increases linearly from 0.4 to 1 about 90 km further eastward (longitude= 0.84° E). Ice thickness also increases from west to east following $h_i = 2(0.1 + e^{-N_x/20})$, where N_x is the number of grid cells in the ~~x-direction~~ x-direction starting from the western border of the ~~ice-covered~~ice-covered domain. Waves radiate from part of the western border of the domain, between 1.2 and 1.8° of latitude, and propagate to the east. The wave spectrum used as forcing at the boundary is extracted at a point south of Svalbard from an Arctic ~~realistic-simulation-using-hindcast~~ performed with WW3 described by Stopa et al. (2016a)for. It covers the period of May 2nd ~~and to~~ 3rd, 2010, during which a storm ~~happened-south of Svalbard-occurred in this particular area~~ (Collins et al., 2015). Here we rotate the spectrum so that the direction with the largest density of wave energy is lined up with our x -axis. Simulations start on April 30th, at 02:00 a.m., and the attenuation processes (scattering, bottom friction and inelastic flexion dissipation) use the same parameterization as in the reference simu-

lation described by Arduin et al. (2018).

2.2 Pan-Arctic configuration

We also make use of the CREG025 configuration (Dupont et al., 2015; Lemieux et al., 2018), which is a regional extraction
5 of the global ORCA025 configuration developed by the Drakkar consortium (Barnier et al., 2006). Although the coupling is
solely between ~~the~~LIM3 and WW3, the configuration here also includes the ocean component of NEMO 3.6 (Madec, 2008).
CREG025 encompasses the Arctic and parts of the North Atlantic down to ~~27~~26^o, and has 75 vertical levels and a nominal
horizontal resolution of $1/4^{\circ}$ ($\simeq 12$ km in the Arctic~~basin~~). Both NEMO-LIM3 and WW3 are run on the same grid. Initial
conditions for the ocean are taken from the World Ocean Atlas 2009 climatology for temperature and salinity. The initial sea
10 ice thickness and concentration are taken from a long ORCA025 simulation performed by the Drakkar Group. Along the lateral
open boundaries, monthly climatological conditions (comprising sea surface height, 3-D velocities, temperature and salinity)
are taken from the same ORCA025 simulation. Regarding the atmospheric forcing, we use the latest version of the Drakkar
Forcing Set (DFS 5.2, which is an updated version of the forcing set described in Brodeau et al., 2010). The choices regarding
the parameterization of the wave-ice attenuation are following the ones made in the *REF* simulation by Arduin et al. (2018).
15 The ~~value of the~~ice flexural strength has however been increased from 0.27 MPa to 0.6 MPa, which is the highest value used
in Arduin et al. (2018). This choice makes sea ice harder to break, and ~~aim at compensating~~ has been made to compensate the
fact that no lateral growth of sea ice is included in our coupled framework.

Three simulations are performed. First we run a simulation based solely on NEMO-LIM3 (referred to as NOT_CPL), cov-
20 ering the period from January 1st, 2002 to the end of 2010, in which the already existing lateral melt parameterization ~~from~~
~~Lüpkes et al. (2012)~~ in LIM3 is activated. The first years of the simulations are allowing for the adjustment of the ocean and
sea ice conditions and we only analyze results from August and September 2010. During that period, the sea ice extent reaches
its annual minimum, providing some fetch for the generation of ~~sea ice, and waves~~, in particular in the Beaufort Sea. The model
sea ice extent during the summer of 2010, and more generally the distribution of the sea ice concentration, compares reasonably
25 well with satellite observations (not shown). Note that this period includes a drop in sea ice concentration in the ~~Central~~central
Arctic, found both in model results and in satellite observations, that has already been documented by Zhao et al. (2018) and
attributed to an enhancement of ice divergence in this region in this particular year. This specific period has also been ~~chosen as~~
~~some storms occurred during it, so that extreme waves selected as it includes a few storm events, so extreme wave~~ conditions
can be investigated. Another simulation (CPL) is initialized from NOT_CPL on August 1st 2010 and run until September 9th
30 2010. After ~~that~~ this date, sea ice extent starts to increase again, and as our FSD distribution does not allow for the refreezing
of ~~the~~ sea ice floes, we cannot ~~represent realistically~~ realistically represent the processes at play during ~~that~~ this period.

Finally, we run a simulation over the same period, based solely on WW3 (referred to as as WAVE), in which the wave model is
forced by sea ice conditions from the NOT_CPL simulation. In order to allow for some spin up for the waves to develop and

break the ice, we remove the first 3 days. In the following, all the results are for the ~~37-days~~ 37-day period between August 4th and September 9th 2010.

3 Implementation of the coupling between the wave and ~~the~~ sea ice models.

The objective of this section is to present the theoretical background and the practical implementation of the coupling between LIM3 and WW3. Fig. 2 shows the principle of the coupling and the variables that are exchanged between the two models. Briefly, LIM3 provides sea ice floe size, thickness and concentration to WW3 in order to estimate the wave attenuation and wave-induced sea ice ~~break-up~~ fragmentation. Note that ~~LIM3 being a multi-category sea ice model, the actual state variable is a~~ in our study, the floe size refers to the caliper diameter of the floes as defined by Rothrock and Thorndike (1984). We refer to sea ice thickness ~~distribution g_h , from which the mean as the cell-average of the~~ sea ice thickness ~~can be defined either by~~ doing a grid-cell average or by doing an ice-cover average. Here we choose to distribution g_h used as a state variable in LIM3. In the coupling, we actually exchange the ice-cover average sea ice thickness, although this choice does not ~~affect significantly~~ significantly affect our results. WW3 then returns the WRS to LIM3, as well as the updated floe size if fragmentation has occurred. LIM3 takes into account the WRS in its ice transport equation, and advects the sea ice and its information on floe size. ~~If break-up~~ This information is carried by a newly implemented FSD, the sea ice concentration being distributed among floe size categories. If fragmentation has occurred in the wave model, ~~floe size is actualized to match the FSD~~ the FSD in LIM3 is re-arranged, transferring sea ice from large floe categories to smaller floe categories. The resulting FSD obeys a power-law similar to the one assumed in WW3. The ~~floe size~~ FSD is then used to estimate lateral melt.

In the following, we describe in more ~~details~~ detail the modifications that have been ~~done~~ carried out in LIM3 and WW3 in order to couple them, and how variables are exchanged between the two models. The coupling allows a new formulation for the sea ice lateral melt in LIM3 (section 3.3).

3.1 Wave Radiative Stress

Waves transport momentum, and when they are attenuated either by dissipation or ~~reflections~~ reflection, this momentum is transferred to ~~the cause of what has caused~~ this attenuation (Longuet-Higgins, 1977). In the case of sea ice, this momentum loss thus acts as a stress that pushes sea ice in the direction of attenuated waves. Following the study of Williams et al. (2017), in which a WRS was implemented in neXtSIM, the WRS $\tau_{w,i}$ is computed as:

$$\tau_{w,i} = \rho_w g \int_0^\infty \int_0^{2\pi} \frac{-S_{ice}(\mathbf{x}; \omega, \theta)}{\omega/k} (\cos \theta, \sin \theta) d\theta d\omega \quad (1)$$

where ρ_w is the water density, g is gravity, ω , θ and k are respectively the radial frequency, direction and wavenumber of waves and $S_{ice}(\mathbf{x}; \omega, \theta)$ is the source term (negative by convention in WW3) corresponding to wave attenuation by sea ice at a given position.

Once estimated by WW3, the WRS is then sent to the sea ice model and added as an additional term in the momentum equation of LIM3 (Rousset et al., 2015):

$$mD_t\mathbf{u} = \nabla \cdot (\underline{\sigma}) + c(\tau_a + \tau_o) + \tau_{w,i} - mf\mathbf{k} \times \mathbf{u} - mg\nabla\eta, \quad (2)$$

in which m is the total mass of ice and snow per unit of area, \mathbf{u} is the ice velocity vector, σ is the internal stress tensor, f is the Coriolis parameter, \mathbf{k} is a unit vector pointing upwards, η is the sea surface elevation, c is the sea ice concentration, and τ_a, τ_o are the atmospheric and oceanic stresses, respectively. In contrast to τ_a and τ_o , $\tau_{w,i}$ doesn't require does not need to be multiplied by c , since the as the wave attenuation estimation in WW3 (and hence the WRS) is already scaled by the sea ice concentration to account for the partial sea ice cover is already accounted for in WW3.

Fig. 1 illustrates the effect of the implementation of the WRS in our simple model. Here, the sea ice thermodynamics is are switched off, so that we only simulated-simulate the effect of waves pushing sea ice. Under the action of waves, the sea ice edge shifts eastward, resulting in an increase of the sea ice concentration (panel b). As the sea ice near the sea ice edge is compacted, it creates a sharp gradient in sea ice concentration and thickness (panels b,ed). When comparing panels (e) and (f), it is clear that wave attenuation also responds to this change of the sea ice properties: waves tend to penetrate further eastward when the sea ice edge retreats to the east, but are then attenuated faster in the compacted sea ice.

3.2 Floe size distribution and sea ice break-upfragmentation

As mentioned earlier, waves can break sea ice and thus impact the sea ice floe size. It is thus required to exchange a FSD therefore necessary to exchange information on floe size between the two models, which can be done by using a FSD. A FSD has been previously implemented in WW3 by Boutin et al. (2018), and is used to estimate the wave attenuation due to inelastic flexure and scattering. Following the work by Toyota et al. (2011) and Dumont et al. (2011), we assume that the FSD in WW3 follows a truncated power law between a minimum floe size, D_{\min} and a maximum floe size, D_{\max} . D_{\min} corresponds to the minimum floe size that can be generated by waves and is of the order of $O(10\text{m})$, while D_{\max} depends on the local waves wave properties and is used to estimate the level of sea ice fragmentation.

There is no FSD included in the standard version of LIM3. However, recent work by Zhang et al. (2015) and Horvat and Tziperman (2015) have has proposed ways to implement a FSD in sea ice models, following what is done for the sea ice thickness distribution (which is a state variable of any multi-category-multi-category sea ice model). Here we start by following the In their study, Horvat and Tziperman (2015) use a joint thickness and floe size distribution in order to represent the evolution of sea ice floes affected by a great variety of processes not necessarily related to waves (i.e welding, refreezing, ridging...). The approach by Zhang et al. (2015) is simpler and computationally cheaper, as it assumes that all floes of a given size have the same ice thickness distribution, allowing the FSD to be treated independently from the sea ice thickness distribution. To do so, they hypothesize that the FSD mostly results from the fragmentation of large unbroken floes randomly yielding floes of any size smaller than the original ones. In this study, we choose to follow the simpler approach of Zhang et al. (2015), distributing-ice

concentration into bins corresponding to different floe sizes by defining a FSD function g_D , as we only consider the effects of wave-induced sea ice fragmentation and lateral melt on the FSD evolution, and our formulation of lateral melt does not depend on sea ice thickness (see section 3.3). Therefore, we can consider the distribution of sea ice thickness and floes independently, defined respectively as:

$$10 \quad \int_h^{h+dh} g_h(h) dh = \frac{1}{A} a_h(h, h+dh) \quad (3)$$

$$\int_D^{D+dD} g_D(D) dD = \frac{1}{A} a_D(D, D+dD) \quad (4)$$

and respecting:

$$\int_0^\infty g_h(h) dh = 1 \quad (5)$$

$$\int_0^\infty g_D(D) dD = 1, \quad (6)$$

- 15 h being the sea ice thickness and D still being the caliper diameter of the floes as defined by Rothrock and Thorndike (1984). In these definitions, A is the total area considered, and a_h and a_D are the areas within A covered by sea ice with thickness between h and $h+dh$ and floes with diameters between D and $D+dD$ respectively. The evolution of the FSD depends on sea ice advection, thermodynamics and mechanical processes, and is given by:

$$\frac{\partial g_D}{\partial t} = -\nabla \cdot (\mathbf{u} g_D) + \Phi_{th} + \Phi_m, \quad (7)$$

- 20 in which \mathbf{u} corresponds to the sea ice velocity vector, Φ_{th} is a redistribution function of floe size due to thermodynamic processes (*i.e* lateral growth/melt), and Φ_m is a mechanical redistribution function associated with processes like fragmentation, lead opening, ridging, and rafting. From a technical point of view, the FSD in LIM3 is implemented as an areal distribution divided into floe size categories. It is advected in the same way as other sea ice tracers like sea ice concentration or thickness.

- 25 In their sea ice model neXtSIM, Williams et al. (2017) have also implemented a FSD that enables the floes to be advected once they have been broken by waves, making the assumption but in a different way than Zhang et al. (2015). Indeed, they assume that the FSD follows a truncated power-law between a minimum and a maximum floe size, similarly similar to the assumption made in WW3. Here we take a similar approach and Thus, in their model, the FSD always obeys a power-law with a constant exponent, and only evolves when sea ice fragmentation results in a reduction of the maximum floe size. Here we combine the approaches of Zhang et al. (2015) and Williams et al. (2017) and implement a FSD in LIM3 that evolves following eq.(7). Yet Eq.7, but that also undergoes a redistribution after each fragmentation event that makes it tend towards the

power-law assumed in WW3. Thus, in contrast to Williams et al. (2017), we do not make any assumption ~~on its shape about~~ the shape of the FSD in general, but ~~the FSD is forced to follow the~~, just as they do, we assume that after being fragmented by waves, the FSD follows a power-law ~~assumed in WW3~~ with a maximum floe size that depends on the local sea state. Our implementation only differs from the one done by Zhang et al. (2015) in the way we have implemented the redistribution: instead of assuming that the broken sea ice is redistributed uniformly among the smaller floes after each fragmentation event (that actually quickly tends towards a power-law distribution with a varying exponent depending on the wave state in their study), our redistribution is set to a power-law with a constant exponent as soon as ~~wave-induced sea ice break-up~~ occurs. This ~~ensure coherence between the FSDs in LIM3 and WW3. We acknowledge that this assumption on the FSD is strong, and as discussed in Roach et al. (2018), it is not a suitable way to proceed when studying the sea ice evolution, since the FSD should evolve freely and observation have regularly shown that power-law distributions are not always followed (e.g. Inoue et al., 2004). However, understanding the details of fragmentation occurs. We justify this choice of redistribution scheme by the fact that fragmentation is a violent process, that can completely change a FSD in time scales of a few minutes~~ to a few hours (see Collins et al., 2015, for the description of such an event). Note that the redistribution of the FSD due to fragmentation transfers sea ice from large floes to smaller floes. Combined with lateral melt, a process that also reduces the floe size, the ~~FSD evolution is beyond the scope of this study, and assuming a power-law FSD is coherent with a distribution caused by a succession of break-up event (Toyota et al., 2011; Dumont et al., 2011)~~ action of waves in our model always reduces the floe size. The details of the mechanical redistribution function Φ_m are mostly following what has been proposed by Zhang et al. (2015) and are given in appendix A.

Now that both models include a FSD, the ~~coupling between the~~ two models can be ~~done coupled~~ in order to represent the effect of the wave-induced sea ice ~~break-up, whose occurrence fragmentation, the occurrence of which~~ in LIM3 is determined depending on information provided by WW3. As mentioned earlier, sea ice ~~break-up fragmentation~~ in WW3 is controlled by local wave properties ~~and break-up, and fragmentation~~ events result in an update of the maximum floe size D_{\max} . It is thus logical to define a similar parameter $D_{\max, \text{LIM3}}$ from the ~~LIM3's FSD, that would FSD of LIM3, that~~ ideally equals D_{\max} . ~~Yet~~ However, estimating $D_{\max, \text{LIM3}}$ is not straightforward. Indeed, our FSD implementation requires that $D_{\max, \text{LIM3}}$ corresponds to the upper limit of the power law followed by the FSD in both WW3 and LIM3, but also that $D_{\max, \text{LIM3}}$ can evolve with the deviations of the ~~FSD in LIM3 's FSD~~ from this power-law under the effects of sea ice advection and thermodynamics. Calling $g_{D, \text{P.L}}$ the distribution corresponding to a FSD following the assumed power-law, we thus define $D_{\max, \text{LIM3}}$ as the greatest value of D for which the following condition applies:

$$\int_D^{\infty} g_D dD \geq k_{D_{\max}} g_{D, \text{P.L}}, \quad (8)$$

in which $k_{D_{\max}}$ is an *ad hoc* parameter allowing the value of $D_{\max, \text{LIM3}}$ to remain unchanged when the FSD slightly deviates away from the assumed power-law (after lateral melt or advection for instance). Setting $k_{D_{\max}}=1$ is ~~a too strong too strong a~~ constraint, and results in noisy D_{\max} distributions, since the smallest change in the FSD after a ~~break-up fragmentation~~ event

results in a change of $D_{\max, \text{LIM3}}$. Values between 0.5 and 0.8 lead to smoother FSDs, but overall the choice of $k_{D_{\max}}$ does not significantly affect our results. In the following, $k_{D_{\max}}$ is set to 0.5.

Floes that have never been broken by waves have no physical reason to follow this truncated power-law. In practice, if we consider a discrete number N of floe size categories, the N^{th} category should represent these unbroken floes, with a different condition to set the value of $D_{\max, \text{LIM3}}$ to D_N (the upper size limit of this category). We thus consider ~~that~~ sea ice in a grid cell ~~can be qualified~~ as unbroken only if most of its floes belongs to this N^{th} category, so that $D_{\max, \text{LIM3}} = D_N$ only if $g_N > 0.5c$,
5 g_N being the value of the FSD function associated to the N^{th} category and c the total sea ice concentration.

In all of our simulations, sea ice is initialized as unbroken everywhere, so that $g_N = c$, and $D_{\max, \text{LIM3}} = D_N$. As soon as wave-induced ~~break-up fragmentation~~ occurs, $D_{\max, \text{LIM3}}$ is updated. To do so, the received value of D_{\max} is rounded up to the upper limit of the category it lies in. $D_{\max, \text{LIM3}}$ is therefore slightly greater than the value received from WW3, with an
10 error that depends on the width of its associated floe size category.

Tests ~~on~~ with the simplified domain were also performed with different number and width of floe categories to investigate the sensitivity of the results to ~~the number and width of floes categories~~ those parameters. This sensitivity remains really small as long as the widths of the categories are smaller than 10 m and ~~that~~ the categories cover a range of floe sizes larger than 300 m. In the following, we ~~used $N=60$~~ use $N=60$ floe size categories, that we define ~~following the conditions~~ as follows:

- 15 – A first category corresponding to the sea ice floes that are already broken but cannot be broken anymore [$D_0 = 8$ m, $D_1 = 13$ m]. D_0 represents the smallest floe size possible in the model, and is set to 8 m in order to agree with the minimum floe size used in LIM3 to estimate lateral melt from the ~~parameterization formula~~ by Lüpkes et al. (2012). D_0 is also of the same order ~~than as~~ the size of the smallest floes that can be generated by wave-induced ~~break-up~~ (Toyota et al., 2011) ~~and therefore fragmentation~~ (Mellor, 1986) ~~and therefore is~~ an acceptable value for the lower limit
20 D_{\min} that the truncated power-law is assumed to follow after wave-induced ~~break-up fragmentation~~.
- 58 categories for which $D_n - D_{n-1} = 5$ m, with $1 \leq n \leq N - 1$.
- A last category representing unbroken floes [$D_{N-1} = 298$ m, ~~$D_N = 1000$~~ $D_N = 1000$ m]. This value of ~~1000 m was~~ $D_N = 1000$ m is set as it is one order of magnitude higher ~~that than~~ the floe size generated by waves (Toyota et al., 2011).

25 We evaluate the effect of this part of the coupling between WW3 and LIM3, as well as the robustness of the implementation of the FSD in LIM3, by ~~performing looking at the same~~ 2 simulations in our idealized configuration, ~~based on as presented in Fig. 1, and comparing an uncoupled WW3 only or the simulation with a coupled WW3-LIM3 model simulation~~ (Fig. 3). ~~Thermodynamics is still~~ Sea ice thermodynamics are switched off in the WW3-LIM3 ~~simulation~~. In the uncoupled WW3 simulation, D_{\max} evolves depending on the sea state, but sea ice thickness and concentration are constant. In the WW3-LIM3
30 ~~coupled simulation, sea ice properties are all evolving as sea ice is pushed by the WRS, and D_{\max} is advected with the FSD~~

in LIM3. The comparison between D_{\max} estimated from the WW3 simulation and $D_{\max, \text{LIM3}}$ from the coupled framework is shown on simulation is shown in Fig. 3(a,b,c). The pattern of broken sea ice is broadly similar in the two simulations (a,b), despite the sea ice retreat due to the WRS in the coupled case. Differences in D_{\max} (Fig. 3c) follow the wave heights height differences already commented on in Fig. 1(e,f). Indeed, the retreat of the ice edge due to the WRS allows for waves to propagate further with less attenuation, thus involving more sea ice break-up-fragmentation and a lower maximum floe size close to the open ocean in the coupled simulation. Further east in the MIZ, the sea ice compacted by the WRS effect generates stronger wave attenuation, and thus less sea ice fragmentation and a greater-maximum-floe-sizes-larger maximum floe size when compared to the not-coupled-uncoupled simulation. Both effects partly compensate, so that the shift in the ice edge position affects-very-little-the-has little effect on the spatial extent of broken ice, which-is-almost-unchanged-between the-two-simulations. Fig. 3d shows the FSD at two locations in the domain. At both locations, the distribution of ice-covered ice-covered area within the different categories agrees very well between LIM3 and the truncated power-law assumed in WW3. The area covered by floes of the smallest possible size in LIM3 is nevertheless greater than it would be if the FSD was exactly following the truncated power-law. This is because floes that have been broken to-down-into the smallest possible size do not contribute to the redistribution (see section A) and accumulate in this category since no lateral growth occurs. Note that a coupled simulation in which advection had been deactivated was also run to ensure that, in a case with unaffected initial sea ice properties, no significant discrepancies were noticeable for both significant wave height and maximum floe size between an-coupled-and-a-not-coupled-a coupled and an uncoupled simulation (not shown).

3.3 Lateral melt

A parameterization to account for the sea ice lateral melt is already implemented in LIM3. Its formulation follows Steele (1992):

$$\frac{dc}{dt} = -w_{\text{lat}} \frac{\pi}{\alpha \langle D \rangle} c, \quad (9)$$

where c is the sea ice concentration, w_{lat} is a-the lateral melt rate, which depends on the difference between sea ice and sea surface temperatures taken from Maykut and Perovich (1987), and α is a coefficient which varies with the floe geometry. By default, $\alpha = 0.66$, which is the average value of the non-circularity of floes obtained by Rothrock and Thorndike (1984). By default, $\langle D \rangle$, which represents the average floe size(referred-to-as-the-caliper-diameter). Based-on-an-number-of-observations, Lüpkes et al. (2012) fitted a relationship between $\langle D \rangle$ and sea ice concentration, so that the lateral melt in the model can be estimated-depending-only-on-, is a function of the sea ice concentration -obtained empirically from observational data by Lüpkes et al. (2012):

$$\langle D \rangle = D_{\min} \left(\frac{c^*}{c^* - c} \right)^\beta \quad (10)$$

where $\beta = 1$ and c^* is introduced to avoid a singularity at $c = 1$ and is defined as:

$$c^* = \frac{1}{1 - (D_{\min}/D_{\min})^{1/\beta}} \quad (11)$$

This relationship finds a value of $\langle D \rangle$ that increases very little from its minimum value (set to D_0) as long as the sea ice concentration remains lower than $\simeq 0.6$ (see Fig. 3 from Lüpkes et al., 2012). ~~It might be a problem far from the ice edge, where divergence can make the ice concentration decreasing to 0.6 or below with an actual floe size being much greater than $\simeq 10$ m.~~ In the following, we refer to this lateral melt parameterization as the parameterization of Lüpkes et al. (2012), although we acknowledge that the work of Lüpkes et al. (2012) only provides a relationship between the average floe size and the sea ice concentration.

In the case of our coupled model, we estimate a FSD, and ~~it thus~~ thus it makes sense to implement a parameterization of the lateral melt that depends explicitly on the FSD rather than ~~the on~~ sea ice concentration. Following the work by Horvat and Tziperman (2015) and Roach et al. (2018), we estimate the lateral melt as:

$$\frac{dc}{dt} = \int_0^\infty \Phi_{th} dD = \int_{0^+}^\infty \underline{-w-2w_{lat}} \left(-\frac{\partial g_D}{\partial D} + \frac{2}{D} g_D \right) dD \quad (12)$$

where Φ_{th} is the change in area covered by floes of a size D due to lateral melt (see Eq. 7). Note that lateral melt for floes in the unbroken category is computed assuming that all the floes have a size D of 1000 m. Note also that Horvat and Tziperman (2015) and Roach et al. (2018) are considering floe radii in their study, while we are working with floe diameters (hence adding a factor of 2 in Eq. 12).

We run two simulations, in which the lateral melt is either estimated from the formulation of Lüpkes et al. (2012), or by our new formulation, which accounts for the ~~actual~~-FSD that is determined by both the sea ice and the wave models (Fig. 4). Here we only activate the lateral melt, and turn off the basal and surface melt. The sea surface temperature is set constant to $T = 0.3^\circ C$. Floe size categories are the same as in section 3.2. In the case of the Lüpkes et al. (2012) parameterization (Fig. 4a), ~~the~~-lateral melt only depends on the sea ice concentration and thus ~~follow~~-follows its distribution. In the second case (Fig. 4b), lateral melt is highly constrained by both the distribution of the sea state and ice properties, and is only significant where the sea ice is broken. Melt rates are overall higher when estimated from the Lüpkes et al. (2012) parameterization, mostly due to the fact that the average floe size in the ~~non-coupled-uncoupled~~ run is very close to D_0 for a wide range of concentrations. Unlike the parameterization that we propose here, the parameterization of Lüpkes et al. (2012) results in a significant lateral melt far from the ice edge, where sea ice is mostly compact and unbroken, which is likely unphysical.

4 Importance of wave-sea ice interactions.

We find that the results are also sensitive to the choice of D_{min} , regardless of the parameterization used. In the case of our FSD, the sensitivity arises from the use of D_{min} to compute the average diameter of the smallest floe size category, which is the category most affected by lateral melt. In order to quantify the sensitivity to the choice of D_{min} , we run similar experiments to the one presented in Fig. 4, varying this time the value of D_{min} (Fig. 5). When using the parameterization of Lüpkes et al. (2012) (Eq. 10 and 11), the volume of sea ice melted laterally roughly doubles when D_{min} is divided by 2

compared to the reference simulation (using $D_{\min} = 8$ m). In the case of our FSD, the sensitivity is still large but greatly reduced, with an increase of only 20% in response to the same change of D_{\min} . Figure 5 also illustrates the strong differences in melted volume between the two parameterizations, with much less lateral melt when computed using the FSD developed here.

10 4 Importance of wave-sea ice interactions

In this section we compare the three simulations performed with the CREG025 configuration described in Section 2.2, in order to quantify the impact of the ~~including the wave-sea ice interactions for the waves~~ coupling on wave, sea ice and ocean surface properties. ~~Remember that although the coupling is only between the wave and the sea ice components, our coupled model includes an ocean component, which is only interacting with the sea ice model but not the wave model. This means that we~~
 15 ~~only consider here the impact that waves may have on the ocean through their impact on the sea ice conditions.~~

To evaluate the impact of waves in the MIZ, we first need to define the MIZ in our model. Various criteria, relying either on sea ice concentration, floe size or the region where waves impact the sea ice floe size, have been previously used to delimit the MIZ (see for instance Dumont et al., 2011; Strong and Rigor, 2013; Sutherland and Dumont, 2018). Here we take the following definition based on the maximum floe size: $0 < \langle D_{\max} \rangle < 700$ m, where ~~$\langle D_{\max} \rangle$~~ $\langle D_{\max} \rangle$ is the average of the maximum
 20 floe size over the ~~studied study~~ period. Physically, it roughly corresponds to the region where sea ice has been broken during a time period that is long enough for the ~~averaged average~~ maximum floe size to ~~be become~~ under 1000 m (which is the limit between the broken and unbroken ice). Note that our results are not dependent on the definition of the MIZ.

4.1 Effect of the coupling at the pan-Arctic scale

4.1.1 Impact on the wave properties

25 First, we examine the ~~significant wave height H_s in differences between~~ the CPL and WAVE simulations, ~~corresponding respectively to the coupled WW3-LIM3 run and a run performed with WW3 in stand-alone mode forced with sea ice properties from NOT_CPL. When looking at the differences in significant wave height H_s (Fig. 6(b,e)). Differences in H_s between the two simulations b), we find that they~~ are small, not exceeding $\simeq 15$ cm on average. Moreover, the two runs exhibit similar patterns of D_{\max} , indicating that the wave-induced ~~break-up fragmentation~~ is similar in the two simulations (Fig. 6fd). Lo-
 30 cally, in the Barents and Greenland seas for instance, the differences ~~of in~~ D_{\max} can be significant, due to the specific ice drift conditions in these regions. Indeed, the overall southward drift of sea ice tends to bring unbroken sea ice from the central Arctic to regions where sea ice is broken up, increasing D_{\max} in the CPL simulation. The signs of the differences in H_s and D_{\max} vary regionally. This might be due to the differences in sea ice concentration and thickness, as the wave attenuation in sea ice is very sensitive to sea ice properties (see for instance Ardhuin et al., 2018). ~~Indeed~~ Certainly, the pattern of the differences in H_s between the CPL and WAVE runs is consistent with the differences in sea ice concentration and thickness between the CPL
 5 and the NOT_CPL simulations (Fig. 7). ~~One should keep in mind that the sea ice conditions from the NOT_CPL run are used~~

as forcing for the WAVE run), with higher waves found in regions where ice is less concentrated and thinner.

4.1.2 Impact on the sea ice and sea surface properties

We now focus on the effect of adding a wave component ~~for on~~ the sea ice properties, by comparing results from the CPL and NOT_CPL simulations. Fig. 7 shows the ~~Pan-Arctic~~ pan-Arctic distribution of the sea ice thickness and concentration averaged over the 37 days considered in the CPL simulation, as well as the differences with the NOT_CPL simulation. These differences are concentrated in the vicinity of the ice edge and ~~exhibits~~ exhibit different signs depending on the location. Positive and negative anomalies tend to compensate, resulting in weak overall ~~difference~~ differences in sea ice extent and volume when averaging over the full Arctic Basin. If we only consider the MIZ, the sea ice volume and area decrease by about 3% and 2%, respectively, between CPL and NOT_CPL (Fig. 8b). Locally, however, these variations can be much larger. In the MIZ of the Beaufort Sea for instance, the relative changes can be as high as 10% for ~~mean-sea-ice-grid cell-average~~ mean-sea-ice-grid cell-average thickness.

There are also ~~difference~~ differences in sea surface properties between the two simulations (Fig. 9), with ~~an average increase~~ average increases in sea surface temperature (SST) and salinity (SSS) in the MIZ ~~of the order~~ as high as $0.5^{\circ}C$ and 0.8 psu locally, respectively. It is worth noting that, in contrast to the sea ice properties, the sign of the differences in SST and SSS tends to be positive, i.e. warmer and saltier in the CPL experiment compared to the NOT_CPL one.

4.1.3 Thermodynamical effect of the coupling

Given that there is no coupling between the ocean and the wave components, the difference in sea surface properties must arise from variations in sea ice conditions, and in particular the sea ice melt, ~~that we investigate and we now investigate this~~ further. Fig. 10(a,b) shows the total sea ice volume ~~melted laterally during the studied~~ loss from lateral melt during the study period in the CPL run as well as ~~its difference with~~ the difference between this and the same quantity from the NOT_CPL run. The sea ice volume melted by lateral melt shows very similar spatial patterns ~~between in~~ the two simulations, although it is estimated from two very different parameterizations (Eq. 9 and Eq. 12), although lateral melt estimated by the parameterization from Lüpkes et al. (2012) tends to be ~~larger in NOT~~ lower in CPL. The difference is substantial, the sea ice volume melted in the MIZ in NOT_CPL being 30% ~~larger than in CPL~~ (lower than in NOT_CPL (Fig. 8a). Another signal is found in the central Arctic, ~~where the value of lateral melt in the NOT_CPL run are small but positive. This is due to the~~ while no lateral melt occurs in this region in CPL. This signal actually arises from the combination of the drop in sea ice concentration that happens in the region in August 2010 (Zhao et al., 2018), ~~resulting in a reduction of the average floe size and the use of the parameterization by Lüpkes et al. (2012) to estimate floe size and resulting lateral melt in NOT_CPL. Indeed, lower sea ice concentration values corresponds to estimated average floe sizes below 100 m when estimated by the formulation of Lüpkes et al. (2012) and thus triggering from the parameterization by Lüpkes et al. (2012), and thus~~ some lateral melt is triggered. In contrast, the absence of waves in the middle of the sea ice pack in ~~the coupled simulation results in unbroken ice~~

5 CPL leaves sea ice unbroken in this region, ~~and therefore no lateral melt preventing lateral melt from occurring~~. An average floe size of $\simeq 100$ m in the middle of the pack seems somewhat unrealistic, and highlights the ~~limitation of the parameterization of Lüpkes et al. (2012) when used in Pan-Arctic configurations. This lateral melt enhancement limitations of estimating the floe size using Lüpkes et al. (2012) parameterization in pan-Arctic configurations.~~ Absence of lateral melt in the central Arctic in ~~the NOT_CPL simulation amplifies the decrease of sea ice concentration in this region. The combination of the sea ice~~
 10 ~~concentration decrease and lateral melt in the NOT_CPL simulation therefore explains the deficit~~ CPL explains the excess in sea ice concentration ~~reported in the central Arctic~~ when compared to the ~~coupled-uncoupled~~ simulation (Fig. 7b). Moreover, the fact that differences in lateral melt between the two simulations ~~being mostly negative, are mostly negative means that~~ it cannot explain the regional patterns found in the distribution of sea ice ~~properties~~ property differences.

15 Fig. 10(c,d) shows the differences in bottom and total ice melt, between the CPL and NOT_CPL simulations. The spatial ~~pattern~~ distributions of the differences in bottom and total ice melt are very similar, meaning that the variations in bottom melt dominate the differences in sea ice melt between CPL and NOT_CPL, although the bottom melt is computed the same way in the two simulations. This result is confirmed by rerunning a coupled and an uncoupled simulation of NEMO-LIM3 while de-activating lateral melt (not shown), which yields differences in total melt distribution almost identical to the ones presented
 20 ~~on in~~ Fig. 10(c,d).

The total melted sea ice volume ~~melted~~, once integrated over the MIZ, increases by 3% between CPL and NOT_CPL, mainly due to the larger volume of sea ice melted laterally in NOT_CPL (Fig. 8a). In parallel, bottom melt slightly decreases by $\simeq 1\%$ between these two simulations. This result ~~does not reflect masks~~ the fact that the regional differences of total melt
 25 are dominated by bottom melt. An explanation is that bottom and lateral melt ~~depend both~~ both depend on the available heat in the surface layer, either directly for bottom melt, or indirectly through lateral melt that depends on the SST. If lateral melt occurs, it removes heat from the surface layer, therefore reducing the bottom melt capacity. ~~Oppositely~~ Conversely, if this heat is not used for lateral melt, it remains available for bottom melt. The overall decrease of bottom melt in the MIZ between CPL and NOT_CPL visible ~~on in~~ Fig. 8a therefore mostly results from the compensation of the increase of lateral melt due to the
 30 change of parameterization, as can be seen ~~on in~~ Figs. 10b and 10c. ~~Actually, in contrast to what was found in previous studies by Zhang et al. (2016); Bennetts et al. (2017); Roach et al. (2018), de-activating completely~~ This compensation mechanism is also reported by Roach et al. (2018) and Bateson et al. (2019) who compare two runs of the sea ice model CICE, one with the standard lateral melt parameterization using a constant floe size of 300 m and one using a FSD (allowing floes smaller than 300 m). In our case, this compensation is strong enough, and completely de-activating lateral melt in both runs ~~(not shown)~~ has a negligible effect on the quantity of melted ice in our simulations ~~(not shown)~~.

4.1.4 Dynamical effect of the coupling

The differences in lateral melt between the CPL and the NOT_CPL runs cannot explain the differences in sea ice and sea surface properties seen ~~on in~~ Figs. 7 and 9. We thus investigate the impact of the WRS on the sea ice conditions and melt.

Fig. 10(e,f) show the mean directions of the wind stress and the WRS in the CPL simulation and the ratio of WRS magnitude ~~on-to~~ wind stress respectively. This ratio is generally low, not exceeding 15% of the wind stress in the eastern Barents Sea, where the WRS reaches its highest magnitude. This is much smaller than the values retrieved from satellite observations in the Southern Ocean, where the wind stress and the WRS can be of comparable ~~magnitudes-magnitude~~ (Stopa et al., 2018a). It is also worth noting that the regions where this relative importance of the WRS compared to the wind is large do not always coincide with regions where differences in sea ice properties are significant (Fig. 7). In the Beaufort Sea for instance, there is substantially less sea ice melt in the CPL simulation than in the NOT_CPL one, although the ratios of WRS over the wind stress are only of the order of a few ~~percents-percent~~ (Fig. 10f). The opposite situation is visible in the Barents Sea, where the high relative influence of the WRS does not result in a significant increase of the sea ice melt when the effect of the waves is included. Therefore, ~~the-amplitude-there is no direct relationship between the intensity~~ of the WRS ~~alone-does-not-allow-to~~ ~~conclude-on-the-mechanism-through-which-the-WRS-impact-sea-ice-melt-and-the-differences-in-sea-ice-and-sea-surface-properties-between-the-coupled-and-uncoupled-simulations.~~ In the Southern Ocean, Stopa et al. (2018a) found that the orientation of the WRS, ~~that-which~~ tends to be orthogonal to the sea ice edge, might explain why WRS ~~might-be-is~~ as important as the wind (that tends to vary ~~much-more-its-direction-in~~ direction much more over time) ~~to-determine-in~~ determining the position of the sea ice edge. Similarly, here, we found that the WRS is very often orientated orthogonally to the ice edge, towards packed ice. ~~It-This~~ is due to the fact that the longer waves encounter sea ice on their path, the more they are attenuated. The direction of propagating waves at a given point in sea ice is then generally imposed by the waves that have ~~traveled-travelled~~ the shortest distance in sea ice. This is particularly visible in some ~~part-parts~~ of the Greenland and ~~the~~-Kara seas, where wind and wave stresses have opposite ~~direction-directions~~ on average. In the Chukchi and the eastern Beaufort seas, the WRS is orthogonal to the wind stress. In contrast, in the Laptev ~~sea~~Sea, the directions of the WRS and the wind stress roughly align, and thus ~~play~~ work together in setting the position of the sea ice edge in the CPL run. However, at the pan-Arctic scale, there is no clear relationship between the WRS direction and the differences in sea ice melt induced by the WRS in the CPL simulation.

The primary effect of the WRS is to push sea ice, modifying the intensity and the direction of the sea ice drift. This impact is significant in the MIZ, where the ~~averaged-average~~ sea ice drift velocity increases by $\simeq 9\%$ between the CPL and the NOT_CPL runs (Fig. 8b). This overall increase of the sea ice velocity can be explained by the fact that both WRS and sea ice drift have a dependency on wind direction. As ~~it~~-was the case for sea ice thickness and concentration, the distribution of the differences in sea ice drift velocity between the two simulations varies strongly depending on the region considered (not shown), but exhibits no clear relationship at the ~~Pan-Arctic-pan-Arctic~~ scale that could explain the differences in sea ice melt induced by the WRS.

In the following we investigate in further ~~details-detail~~ the wave-sea ice interactions in two regions during storms. Indeed, although the differences between the CPL and NOT_CPL run at the pan-Arctic scale ~~remains-remain~~ small, it is clear that the way the waves can influence the sea ice and the ocean surface would depend on the local properties of ~~wave~~the waves, wind, sea ice and ocean surface.

4.2 Regional impacts of ~~waves-sea~~ wave-sea ice interactions during storm events

4.2.1 Case 1: Storm in the Beaufort Sea (16-17 August 2010)

We first focus on a storm event that occurred near the MIZ in the Beaufort Sea on 16-17 August 2010 (Figs. 11(a,b,c) and 12(a,e)). During the storm, waves and winds are oriented ~~toward the North-West on the West~~ towards the north-west on the west side of the domain, but ~~toward the West on the East~~ towards the west on the east side. Wave height and wind speed are reaching up to 3 m and 12 m/s (Fig. 11a,b), respectively, while they do not exceed 1 m and 7 m/s during the 3 days preceding the storm (not shown). Before the event, the south Beaufort Sea is ice-free, and the position of the sea ice edge (defined at the 15% sea ice concentration contour) is highly irregular, with the presence of an ice tongue centered around 72°N and 155°W, that is exposed upwind ~~(and waves)~~ on its eastern side but downwind on its western side during the storm. This sea ice tongue is composed of relatively thick ice ($\geq 1\text{m}$ $> 1\text{m}$). During the storm, sea ice breaks all over the ice tongue in the western part of the domain, but not further than $\simeq 40$ km after the sea ice edge. Both the waves and the wind stresses push the ice to the west (Fig. 11b,c), accelerating the drift that is directed north-west (Fig. 12a,c), as ~~it~~ was already the case before the storm (not shown). The wave action is particularly effective at the location of the sea ice tongue, where the WRS has an amplitude comparable to the wind stress over sea ice (Fig. 11c). As a consequence, the sea ice drift is substantially accelerated (Fig. 12c). ~~Considering the~~ The effect of the waves results in large changes of the sea ice thickness pattern (when comparing the CPL and NOT_CPL runs), with a decrease on the eastern part of the tongue but an increase on the western part (Fig. 12g). Outside of the sea ice tongue, the differences between the simulations are very small, likely because of the sharp sea ice thickness gradient opposing internal resistance to deformation (Fig. 12e), and the relative small effect of the WRS compared to the wind stress (Fig. 11c).

The differences ~~of in~~ in sea ice properties around the sea ice tongue between the two runs also result in changes in SST and SSS, with ~~increase~~ increases around 1°C and ~~1psu~~ 1 psu, respectively, on the eastern side of the sea ice tongue, and a decrease of roughly the same magnitude on the western side (Fig. 13c,g). ~~This differences arises~~ These differences arise from changes in sea ice melt, as differences ~~of in~~ in the total heat flux at the sea surface (Fig. 14a) are largely determined by bottom melt (Fig. 14b), the lateral melt contribution being one order of magnitude lower in this case. On the eastern side of the sea ice tongue, waves tend to push the sea ice away from the edge in the CPL run, and thus away from surface waters with warmer SST, resulting in a smaller amount of heat in the surface layer available for bottom melt. As the sea ice melt decreases, it also reduces the amount of freshwater received by the ocean surface, resulting in larger SSS. On the western side of the south end of the ice tongue, where the sea ice is thicker in the CPL run than in the NOT_CPL one, the opposite effect happens, ~~eventually~~ explaining the lower SST and SSS values. One should note that the effects of this storm are particularly strong, due to the specific conditions before the storm, with warm waters brought very close to the sea ice edge during the storm (not shown).

In our model, bottom melt arises from heat fluxes determined by two distinct processes: (i) a conductive heat flux, ~~which intensity~~ the intensity of which is controlled by the difference between sea ice temperature and SST, and (ii) a turbulent heat flux in the surface layer, which depends on both the SST and the shear between the sea ice and the sea surface currents. The inclusion of the ~~effect of the waves and the~~ WRS could in principle ~~modified the total bottom melt~~ affect the turbulent heat flux through its effect on the sea ice drift, but it is not the case here, suggesting that the deficit of sea ice melt on the eastern side of

the sea ice tongue in the CPL run is therefore due to the combination of colder SST and ~~the~~ sea ice reduction.

10 4.2.2 Case 2: Storm in the Barents Sea (16-17 August 2010)

The storm that we just examined in the Beaufort Sea occurred on the same date ~~than~~ as a second and stronger storm in the Barents Sea, with wave heights up to 5 m and south-westward winds reaching $\simeq 15$ m/s on average over the two days (bottom panels of Fig. 11d,e). In the CPL run, waves ~~break-up~~ fragments sea ice over a very large area (Fig. 12f). Similarly to what we see in the Beaufort Sea, the mean direction of propagation of the waves aligns with the direction of the wind over the ice-free
15 ocean, and is rotated orthogonally to the gradient in sea ice thickness once in the sea ice pack (Fig. 11d). The transition is however much smoother here than in the Beaufort Sea as the gradient is much weaker (Fig. 12f). In the CPL run, sea ice is drifting southward (Fig. 12b), with a slight deviation from the wind direction, and speeds twice ~~larger than~~ as large as in the Beaufort Sea, due to stronger winds and thinner and less concentrated sea ice.

20 In contrast to the ~~effect~~ effects of the storm in the Beaufort Sea, the WRS in the CPL run reaches large values (Fig. 11f). Indeed, the strong storm generates ~~very high waves of which attenuation induces WRS~~ high waves, inducing a WRS as large as the wind stress close to the sea ice edge ~~as large as the wind stress where most of the attenuation takes place~~, although the WRS does not align with the direction of the wave propagation in ice. This is due to the low sea ice concentration in this region that allows for wave generation ~~on~~ over a large region, even if partially ice-covered. The attenuation of these short in-ice generated
25 waves dominates the WRS that is therefore aligned with the wind direction, thus accelerating the ice drift, especially close to the ice edge (Fig. 12d).

The differences in sea ice drift between the CPL and the NOT_CPL runs also result in differences in bottom melt (Fig. 14d), and more specifically ~~of~~ in the part associated with the turbulent heat flux (not shown). This increase of the turbulent heat flux,
30 which occurs in the Barents Sea but not in the Beaufort Sea, can be explained by the larger ice drift velocities driven by the WRS, which intensify the shear between the sea ice and the ocean, and therefore the turbulence in the surface mixed layer. The differences in sea ice drift between the two runs also result in changes of the conductive heat flux. ~~Yet~~ However, in the Barents Sea, the sea ice thickness and concentrations are lower than in the Beaufort Sea while the sea ice temperature is ~~overall~~ higher higher overall (not shown). This results in only moderate differences of the conductive heat flux between the CPL and ~~the~~ NOT_CPL runs.

The differences in SST and SSS exhibit similar ~~pattern than~~ patterns to the differences in heat flux (Fig. 13d,h and Fig. 14c), but the magnitude of the differences are much weaker than in the Beaufort Sea, not exceeding a few tenths of $^{\circ}\text{C}$ and psu
5 for SST and SSS respectively. These small differences can be explained by two causes: (i) the small differences of sea ice properties between the two simulations result in small changes in melt, and (ii) the initial state before the storm is also different with higher SST and SSS in CPL (not shown). This difference in the initial state can be related to previous ~~waves~~ wave and

wind conditions(~~not shown~~): low wind speeds are not sufficient to generate waves in the MIZ, implying that the WRS must be directed northward in the same direction as the propagating waves. It therefore compacts the sea ice edge, and thus reduces sea ice melt in the MIZ in the CPL run. As seen in the Beaufort Sea case, this in turn leads to higher SST and SSS values in the vicinity of the ice edge.

4.2.3 What determines the impact of the waves?

From these two particular cases we suggest a generalization of the mechanisms by which the waves can impact the sea ice and ocean properties in the MIZ. It is based on a simple principle: if sea ice is moved towards warmer water, it tends to melt more, and *vice versa*. The direction of the WRS compared to the orientation of the sea ice edge is thus fundamental if we are to understand the impact of the waves. In compact sea ice, waves are quickly attenuated and the direction of the WRS is generally towards the packed ice, thus impeding part of the sea ice melt and increasing the SST and SSS (Fig. 9). In regions where the sea ice is less concentrated and thinner, waves can be generated locally, so that the WRS aligns with the wind, whose direction determines the impact of the WRS (enhanced melt for off-ice wind and reduced melt for on-ice wind). Another key factor determining the impact of the WRS ~~onto~~on sea ice is the internal stress of sea ice (a.k.a the rheology; see Eq.2). The impact of the WRS is larger in regions of the MIZ where the sea ice is thin and ~~low concentrated~~has low concentration, as the internal stress tends to be negligible (Hibler III, 1979), making the sea ice easier to deform and to drift freely. Close to the sea ice edge in the Barents Sea for instance, the WRS in storm-induced high ~~waves-wave~~ conditions can be larger than the wind stress, strongly accelerating the sea ice drift towards the open ocean, which also ~~result~~results in an increase of the ~~ice/ocean~~ice-ocean shear, enhancing the turbulent heat flux under sea ice and thus the sea ice melt.

5 Discussion and conclusion

The goal of this study was to examine the wave-sea ice interactions in the MIZ of the Arctic Ocean during the melt season, as these processes are thought to be important for determining the sea ice conditions but are not accounted for in the state-of-the-art sea ice models. To that aim, we have developed a model framework, coupling the wave model WW3 with a modified version of the ocean/sea ice model NEMO-LIM3. The coupled model was then used to examine two aspects of the wave-sea ice interactions: (i) the impact of the WRS on the sea ice drift in the MIZ, and (ii) the effects of using the wave-induced sea ice ~~break-up on the sea ice~~fragmentation to estimate lateral melt. The WRS tends to compact the ice edge and thus reduces the total sea ice melt in the MIZ. Yet, its overall impact on the MIZ sea ice area and volume remains limited (Fig. 8b). However, it has a visible impact on sea ice drift velocity, accelerating it by $\simeq 9\%$. Compared to the use of ~~Lüpkes et al. (2012) parameterization~~the parameterization of Lüpkes et al. (2012) to estimate the floe size used in lateral melt, our parameterization strongly reduces the amount of sea ice melted laterally. It is however mostly compensated by an increase of bottom melt, similar to what was found by Bateson et al. (2019). As a result, the effects on sea ice and sea surface properties can be locally substantial, and even more substantial during storms, as illustrated by the case studies in the Beaufort and Barents seas. As the storminess in

the Arctic region is expected to increase in the future (Day et al., 2018; Day and Hodges, 2018), generating higher and more energetic waves more frequently (Khon et al., 2014), the wave-sea ice interactions might become a dominant signal controlling the dynamics of the MIZ.

10

In the MIZ, waves push sea ice as they are attenuated, ~~modifying locally~~ locally modifying the position of the sea ice edge through a modulation of the magnitude and timing of the sea ice melt, which ~~result~~ results in significant changes of the SST and SSS. Although the impact at the pan-Arctic scale remains limited, the case studies of storms in the Barents and Beaufort seas ~~shows that it~~ show how this modulation can be locally and intermittently important. Results from our simple configuration have also revealed that the WRS could strongly modulate the position of the sea ice edge. Yet, except very locally in response to strong storms, the position of the pan-Arctic sea ice edge simulated by our realistic configuration appears to be insensitive to the effect of the wave. This is likely because the position of the sea ice edge in a ocean-sea ice model is primarily determined by the atmospheric forcing and the bulk formulae, and is in particular strongly ~~tight-tied~~ to the position of the sea ice edge in the atmospheric reanalysis (Chevallier et al., 2017). The ~~effect~~ effects of the waves on sea ice simulated by our coupled model are likely underestimated, and should be re-assessed in future studies based on a fully coupled model that includes an atmospheric component.

15

20

We ~~also have~~ have also tested two parameterizations of the lateral melt, based either on wave-induced ~~break-up~~ fragmentation information or solely on a scaling between the size of the floes and the sea ice concentration, following Lüpkes et al. (2012). ~~In both cases, the~~ We first acknowledge that the effect of our lateral melt parameterization depends strongly on the FSD, and hence on the choices and assumptions made regarding its implementation. For instance, our redistribution scheme associated with sea ice fragmentation assumes that successive fragmentation events lead to a power-law FSD. This assumption is made based on the observations analyzed by Toyota et al. (2011), that only sample a small area in time and space, and their findings may not be applicable globally. More generally, Roach et al. (2018) recommend avoiding forcing the shape of the distribution, as the analysis of observations have revealed that FSDs do not always follow power-law distributions (e.g. Inoue et al., 2004). They foster the use of alternative approaches, such as the one developed by Horvat and Tziperman (2015). However, results from laboratory experiments focusing on the fragmentation of sea ice by waves by Herman et al. (2018) indeed suggest power-law distributions for the smallest floe sizes generated, similarly to what was found by Toyota et al. (2011) for the small floes regime. This justifies the choice made in the present study. More generally, large uncertainty remains regarding the key parameters governing the FSD redistribution (coming from waves or sea ice properties), and more dedicated observations will be needed in the future to better constrain FSD in models.

25

30

35

Regardless of the choices made for the implementation of the FSD, the effect of the lateral melt for both formulations remains limited as any change of lateral melt tends to be compensated by an opposite change of bottom melt. The effect might however become more important if longer simulations were performed. Indeed, Zhang et al. (2016) found that, over a year, the lateral melt could ~~affect significantly~~ significantly affect the sea ice thickness. In their case, a FSD-based parameterization

5

was used (similar to the one we introduced in our coupled model), but the effect of the wave-induced ~~break-up fragmentation~~ on the FSD was only crudely parameterized, resulting ~~in most likely in an overestimation of~~ lateral melt in the central Arctic ~~most likely over-estimated~~ (as this is the case when using the parameterization of Lüpkes et al., 2012). Adding a FSD in their sea ice model, ~~?-found~~ Roach et al. (2018) found a large impact on ~~the~~ sea ice concentration in the MIZ and sea ice thickness everywhere in the Arctic after 20 years of simulation, and suggested that the ~~difference-differences~~ found in the central Arctic ~~results-result~~ from a redistribution of the heat used for lateral melt instead of bottom melt, similar to what happens in our model over a shorter timescale. One should also remember that the studies of Zhang et al. (2016) and ~~?-were-aiming-at representing~~ Roach et al. (2018) aimed to represent the evolution of floes ~~larger than 1000 m with sizes ranging from a few cm to roughly 1 km~~ on long time scales, whereas we focus on the important processes for wave-sea ice interactions and make the assumption that unbroken floes have ~~an-a~~ uniform floe size set to 1000 m ~~in-order-to-focus-on-the-important-processes-for-the wave-sea-ice-interactions~~. Therefore we do not expect any impact of the lateral melt in regions that are not impacted by waves. Note also that we evaluate the impact of changing the lateral melt parameterization by comparing two simulations for which lateral melt depends on a varying floe size, either deduced from the FSD or estimated from the sea ice concentration using the parameterization suggested in Lüpkes et al. (2012). It differs from Zhang et al. (2016) who compare their FSD-model with a reference run without lateral melt, and from Roach et al. (2018) who use a constant floe size of 300 m in their lateral melt parameterization. This might partly explain the discrepancies between our respective conclusions.

Among the wave-sea ice interaction processes considered in this study, we ~~found-find~~ that the dynamical effect of the waves (the WRS) has a larger impact ~~than the thermodynamical one (through the additional lateral source melt) on sea ice conditions and sea surface properties than the modulation of lateral melt by sea ice fragmentation~~. Our simulations were however limited to only a few weeks during the melting season and it is unclear if ~~that-the~~ result would hold if longer timescales were considered. ~~To make progress on~~ In order to answer this question, we would need to implement a parameterization that ~~account accounts~~ for the refreezing of ~~the~~ floes, through lateral growth and welding. A first parameterization of ~~that-this~~ kind has been very recently developed by Roach et al. (2018). We also anticipate that running a simulation over longer time ~~period-periods~~ would highlight new impacts of the WRS. Indeed, observations have revealed that heat stored during ~~the~~ melt season below the mixed layer can significantly affect ~~the~~ sea ice growth the following year (Jackson et al., 2010; Timmermans, 2015). In regions where the WRS contributes to ~~reduce-reducing~~ the ice melt, an excess of summer heat could likely accumulate under the mixed layer, possibly modulating the future evolution of the sea ice melt and growth. Recently, Smith et al. (2018) ~~have-for instance,~~ for instance, observed that a large amount of heat stored under the mixed layer could be released to melt sea ice during a storm. The significant changes of SST and SSS found locally over 37 days also highlight that wave-sea ice interactions should be considered when trying ~~the-to~~ forecast the Arctic sea ice conditions on short ~~timescale-timescales~~ (up to a few weeks), as these surface ocean changes can greatly affect melting and refreezing conditions.

The coupling developed in ~~the-present-this~~ study marks a valuable new step ~~toward-towards~~ an improved representation of waves and sea ice interactions in models, which might improve the representation of the dynamics ~~of-in~~ the MIZ. Yet, our

coupling relies on a number of assumptions, which are most likely leading to an underestimation of the impact of the ~~wave~~ waves on the ocean and sea ice conditions. For instance, in our coupling, the sea ice rheology is unaffected by fragmentation, which is unlikely to be the case in reality (McPhee, 1980). Moreover, the sea ice model used here does not retain any memory of the past sea ice conditions, while ~~wave-waves~~ would most likely ~~affect-differently~~ have a different effect on sea ice that has
15 been previously broken (Langhorne et al., 1998). Developing a similar coupling using a model that ~~consider~~ considers a state variable accounting for the previous sea ice conditions (such as ~~the state variable ‘damage’ included in the~~ in the neXtSIM sea ice model ~~neXtSIM~~ (Rampal et al., 2016; Williams et al., 2017)) would probably reveal new mechanisms via which waves can modulate the ocean and sea ice conditions in the MIZ.

20 Finally, the coupling we have developed here is also only considering the interactions between ~~wave-waves~~ and sea ice, without any direct coupling with the ocean and the atmosphere. Yet, we know that wave dissipation would also likely impact the mixed layer, by enhancing turbulence (Couvelard et al., Submitted), and eventually modulate the rate of sea ice melt and formation (Martin and Kauffman, 1981; Rainville et al., 2011; Lee et al., 2012; Smith et al., 2018). Similarly, the effect of the waves is probably damped due to the lack of feedbacks with the atmosphere (Khon et al., 2014). Future coupling should
25 include some of these features in order to fully capture the complexity of the MIZ dynamics.

Code and data availability. Will be made available before final submission

Appendix A: Floe size redistribution in the sea ice model LIM3

Here we provide the details of the calculation and implementation of the FSD, and in particular of the mechanical redistribution function Φ_m that accounts for processes such as sea ice fragmentation, lead opening, ridging, and rafting. Following Zhang
30 et al. (2015), Φ_m can be divided into 3 terms as $\Phi_m = \Phi_o + \Phi_r + \Phi_f$ where Φ_o represents the creation of open water, Φ_r represents sea ice ridging and rafting, and Φ_f represents the wave-induced ~~floes-floe~~ fragmentation. Here we compute Φ_o and Φ_r in a similar way to Zhang et al. (2015), assuming that all the floes of different sizes have the same ice thickness distribution, so that changes in sea ice concentration due to open water creation or ridging ~~affects-affect~~ all floes equally. As a result, the shape of the FSD and its evolution are independent from these two terms.

Assuming that, in a given grid cell, sea ice fragmentation does not induce any change of the sea ice concentration, Φ_f can
5 be written as (Zhang et al., 2015):

$$\Phi_f = -Q(D)g_D(D) + \int_0^\infty Q(D')\beta(D',D)g_D(D')dD' \quad (\text{A1})$$

where D is the floe size, $Q(D)$ is a redistribution probability function characterizing which floes are going to be broken depending on their size, and $\beta(D',D)$ is a redistribution factor quantifying the fraction of sea ice concentration transferred from one floe size to another as ~~break-up~~ fragmentation occurs. Φ_f is thus used to transfer sea ice concentration from large

10 floes to smaller floes. To ensure the conservation of sea ice area during fragmentation, β must respect (Zhang et al., 2015):

$$\int_0^{\infty} \beta(D', D) dD = 1 \quad (\text{A2})$$

In the absence of a wave model to simulate the sea state, Zhang et al. (2015) ~~has defined~~ β so that it ~~redistributes uniformly~~ uniformly redistributes the sea ice concentration of the large broken floes into the smaller floe ~~sizes-size~~ categories of the FSD. Their redistribution probability function $Q(D)$ thus assumes that a constant fraction of the sea ice cover is broken by
 15 waves during each ~~break-up fragmentation~~ event. Their definition of $Q(D)$ also ensures that larger floes contribute more to the redistribution than smaller floes.

In our coupled model, sea ice ~~break-up fragmentation~~ is initially computed by WW3 (for details see Boutin et al., 2018), and accounts for the sea state variability. In WW3, the FSD resulting from wave-induced ~~break-up fragmentation~~ is assumed to follow a truncated power-law between a minimum (D_{\min}) and a maximum (D_{\max}) floe size. For consistency, the FSD in
 20 LIM3 after a given ~~break-up fragmentation~~ event must follow the same power-law, defined for D taken in $[D_{\min}, D_{\max}]$ assuch as, for a given floe size D_* also taken in $[D_{\min}, D_{\max}]$:

$$P(D > D_*) = K D_*^{-\gamma}, K \in \mathbb{R} \quad (\text{A3})$$

$$p(D) = -K\gamma D^{-\gamma-1} \quad (\text{A4})$$

where $P(D > D_*)$ is the probability of having $D > D_*$, and $p(D)$ is the associated probability density. In WW3, a ~~break-up~~ fragmentation event occurs if, firstly, waves with a wavelength λ ~~applies-apply~~ a strain on sea ice greater than a given threshold, and secondly if $\lambda/2$ which is assumed to be the value of the new maximum floe size is lower than the current D_{\max} value in the wave model (Dumont et al., 2011). Therefore, a ~~break-up fragmentation~~ event in WW3 corresponds to a decrease of D_{\max} .

As detailed in section 3.2, we define a maximum floe size in LIM3, $D_{\max, \text{LIM3}}$, that is compared to the value of the maximum floe size received from WW3, $D_{\max, \text{WW3}}$. Initially, ice is unbroken and $D_{\max, \text{LIM3}} = D_{\max, \text{WW3}}$. If ~~break-up fragmentation~~ has occurred in WW3, then we have $D_{\max, \text{WW3}} < D_{\max, \text{LIM3}}$. In this case, $D_{\max, \text{LIM3}}$ must be updated to the $D_{\max, \text{WW3}}$ value, and Φ_f must be computed so that it forces the FSD in LIM3 to match the FSD assumed in WW3.

5 In practice, in LIM3, we define a given number N of floe size categories, such that each floe size category $n \in [0, N]$ represents the floes with sizes in $[D_{n-1}, D_n]$. D_0 and D_N are the minimum and the maximum floe size possible in the model, respectively. D_N aims ~~at-representing-to represent~~ floes that have not been broken by the waves. In WW3, the size of unbroken floes is set to 1000 m, and we thus also set $D_N = 1000\text{m}$ for consistency. Regarding the minimum floe size resulting from wave induced ~~break-up fragmentation~~, we set D_{\min} to 8 m, which is the value of the minimum floe size used in the parameterization
 10 of lateral melt implemented in LIM3. This value is close to choices ~~done-made~~ in previous studies (see Williams et al., 2013; Bennetts et al., 2017). If ~~break-up fragmentation~~ occurs, the update of $D_{\max, \text{LIM3}}$ is done as follows:

$$\begin{cases} D_{n^*-1} < D_{\max, \text{WW3}} \leq D_{n^*} \\ D_{\max, \text{LIM3}} = D_{n^*} \end{cases} \quad (\text{A5})$$

Here n^* is the index of the floe size category in which the maximum floe size received from the wave model lies in. $D_{\max, \text{LIM3}}$, the maximum floe size in the sea ice model is thus set equal to D_{n^*} , the upper bound of the n^* -th category. To force the FSD to follow this power-law during the computation of the mechanical redistribution term Φ_f , in LIM3 we introduce changes in the computation of β and $Q(D)$. When using N floe size categories, the redistribution equation (A1) becomes:

$$\Phi_{f,n} = -Q_n g_n + \sum_{m=1}^N \beta(m,n) Q_m g_m, \quad m \in [0, N] \quad (\text{A6})$$

Following Zhang et al. (2015), the redistribution factor $\beta(m,n)$ must respect Eq.A2. $\beta(m,n)$ should also allow to switch from completely unbroken ice to a truncated power-law distribution with lower limit D_0 and upper limit $D_{\max, \text{LIM3}}$ if break-up occurs. Finally, $\beta(m,n)$ must finally ensure that floe size can only decrease during the fragmentation. To do so, $\beta(m,n)$ is defined as:

$$\begin{cases} \beta(m,n) = \frac{D_n^{2-\gamma} - D_{n-1}^{2-\gamma}}{\min(D_{n^*}, D_m)^{2-\gamma} - D_0^{2-\gamma}} & \text{if } m \geq n \text{ and } n \leq n^* \\ \beta(m,n) = 0 & \text{otherwise} \end{cases} \quad (\text{A7})$$

With this choice of $\beta(m,n)$, the FSD of each floe size category $n < n^*$ is equal to the distribution function derived from the power-law assumed in WW3 ($g_{n,\text{P.L.}}$), given by:

$$g_{n,\text{P.L.}} = c \frac{\int_{D_{n-1}}^{D_n} D^2 p(D) dD}{\int_{D_0}^{D_{\max}} D^2 p(D) dD} = c \frac{D_n^{2-\gamma} - D_{n-1}^{2-\gamma}}{D_{\max}^{2-\gamma} - D_0^{2-\gamma}}, \quad (\text{A8})$$

c being the sea ice concentration.

If sea ice in a given grid cell has already been broken, the FSD may have deviated from the truncated power-law distribution (due to advection or melting). If break-up fragmentation occurs again at a latter-later model time step, we force the FSD to be reset to the power-law assumed in WW3, by adjusting the fraction of each floe size category contributing to the redistribution through the value Q_n . This ensures that the FSD in LIM3 and WW3 are identical. After a break-up fragmentation event, $D_{\max, \text{LIM3}}$ is the new maximum floe size in LIM3. The sea ice contained in floe size categories associated with floes larger than $D_{\max, \text{LIM3}}$ is therefore entirely redistributed into smaller floe size categories by setting:

$$Q_n|_{n > n^*} = 1. \quad (\text{A9})$$

The smallest floe size category (*i.e* $D \in [D_0, D_1]$) does not contribute to the floe size redistribution, assuming that this category accounts for floes too small to be broken by waves (Toyota et al., 2011). It therefore forces $Q_1 = 0$. For a given floe size category n , we define $\Delta g_{th,n}$ as the difference between the actual and theoretical values of the FSD for this floe size category ($\Delta g_{th,n} = g_n - g_{n,\text{P.L.}}$), and the theoretical value is given by the truncated power-law between D_0 and $D_{\max, \text{LIM3}}$. After the redistribution of floes between categories, $\Delta g_{th,n}$ needs to be zero, which is achieved through the adjustment of Q_n in order

to obtain $\Phi_{f,n} = \Delta g_{th,n}$. The following system thus needs to be solved:

$$\left\{ \begin{array}{l} \Phi_{f,2} = (-1 + \beta_{2,2})Q_2g_2 + \beta_{3,2}Q_3g_3 + \dots + \beta_{n^*,2}Q_{n^*}g_{n^*} + \sum_{n>n^*}^N \beta_{n\geq n^*,2}g_n \\ \Phi_{f,3} = (-1 + \beta_{3,3})Q_3g_3 + \beta_{4,3}Q_4g_4 + \dots + \beta_{n^*,n^*}Q_{n^*}g_{n^*} + \sum_{n>n^*}^N \beta_{n\geq n^*,3}g_n \\ \dots \\ \Phi_{f,n^*} = (-1 + \beta_{n^*,n^*})Q_{n^*}g_{n^*} + \sum_{n>n^*}^N \beta_{n\geq n^*,n^*}g_n, \end{array} \right. \quad (A10)$$

This system consists in a triangular matrix in which all diagonal terms are non-zero. It is solved by doing:

$$\left\{ \begin{array}{l} Q_{n^*} = \max \left(0, \frac{\Delta g_{th,n^*} - \sum_{n>n^*}^N \beta_{n\geq n^*,n^*}g_n}{g_{n^*}(\beta_{n^*,n^*} - 1)} \right) \\ \dots \\ Q_2 = \max \left(0, \frac{\Delta g_{th,2} - \sum_{n>2}^N Q_n \beta_{n,2}g_n}{g_2(\beta_{2,2} - 1)} \right) \end{array} \right. \quad (A11)$$

- 20 The constraint $Q_n > 0$ ensures that the redistribution can only be done ~~toward~~towards categories containing smaller floe ~~sizes~~sizes. This constraint thus implies that, in the case where $\Delta g_{th,n} > 0$, the FSD in LIM3 is reset to the truncated power-law only if there is enough sea ice in large ~~floes~~floe categories to be redistributed into smaller ~~floes~~floe categories. Besides, setting $Q_1 = 0$ means that the sea ice concentration associated with the smallest floe size category is never redistributed. In the absence of lateral growth, a succession of ~~break-up~~fragmentation events leads to an accumulation of floes in this category, deviating
- 25 the FSD from the theoretical power-law for floe sizes between D_0 and D_1 (see Fig. 3).

Competing interests. The authors declare no competing interests.

- Acknowledgements.* G.B. and F.A. are supported by DGA, ANR grants ANR-14-CE01-0012 MIMOSA, ANR-10-LABX-19-01, EU-FP7 project SWARP under grant agreement 607476, ONR grant number N0001416WX01117. Part of this work has been carried out as part of the Copernicus Marine Environment Monitoring Service (CMEMS) ArcticMix and WIZARd projects. CMEMS is implemented by Mercator
- 30 Ocean in the framework of a delegation agreement with the European Union. We thank Martin Vancoppenolle for ~~its~~his valuable help as well as Verena Haid and Xavier Couvelard for their ~~precious~~significant assistance in setting up the coupled framework.

References

- Aksenov, Y., Popova, E. E., Yool, A., Nurser, A. G., Williams, T. D., Bertino, L., and Bergh, J.: On the future navigability of Arctic sea routes: High-resolution projections of the Arctic Ocean and sea ice, *Marine Policy*, 75, 300–317, 2017.
- 35 Ardhuin, F., Sutherland, P., Doble, M., and Wadhams, P.: Ocean waves across the Arctic: attenuation due to dissipation dominates over scattering for periods longer than 19 s, *Geophys. Res. Lett.*, 43, <https://doi.org/10.1002/2016GL068204>, 2016.
- Ardhuin, F., Chapron, B., Collard, F., Smith, M., Stopa, J., Thomson, J., Doble, M., Wadhams, P., Blomquist, B., Persson, O., and Collins, III, C. O.: Measuring ocean waves in sea ice using SAR imagery: A quasi-deterministic approach evaluated with Sentinel-1 and in situ data, *Remote Sensing of Environment*, 189, 211–222, 2017.
- Ardhuin, F., Boutin, G., Stopa, J., Girard-Ardhuin, F., Melsheimer, C., Thomson, J., Kohout, A., Doble, M., and Wadhams, P.: Wave Attenuation Through an Arctic Marginal Ice Zone on October 12, 2015: 2. Numerical modeling of Waves and Associated Ice Break-Up, *Journal of Geophysical Research: Oceans*, <https://doi.org/10.1002/2018JC013784>, 2018.
- 5 Asplin, M. G., Galley, R., Barber, D. G., and Prinsenber, S.: Fracture of summer perennial sea ice by ocean swell as a result of Arctic storms, *J. Geophys. Res.*, 117, C06 025, <https://doi.org/10.1029/2011JC007221>, 2012.
- Barnier, B., Madec, G., Penduff, T., Molines, J.-M., Treguier, A.-M., Sommer, J. L., Beckmann, A., Biastoch, A., Böning, C., Dengg, J., Derval, C., Durand, E., Gulev, S., Remy, E., Talandier, C., Theetten, S., Maltrud, M., McClean, J., and Cuevas, B. D.: Impact of partial steps and momentum advection schemes in a global ocean circulation model at eddy-permitting resolution, *Ocean Modelling*, 56, 543–567, <https://doi.org/10.1007/s10236-006-0082-1>, 2006.
- 10 Bateson, A. W., Feltham, D. L., Schröder, D., Hosekova, L., Ridley, J. K., and Aksenov, Y.: Impact of floe size distribution on seasonal fragmentation and melt of Arctic sea ice, *The Cryosphere Discussions*, 2019, 1–35, <https://doi.org/10.5194/tc-2019-44>, <https://www.the-cryosphere-discuss.net/tc-2019-44/>, 2019.
- 15 Bennetts, L., O’Farrell, S., and Uotila, P.: Brief communication: Impacts of ocean-wave-induced breakup of Antarctic sea ice via thermodynamics in a stand-alone version of the CICE sea-ice model, *The Cryosphere*, 11, 1035–1040, <https://doi.org/10.5194/tc-11-1035-2017>, 2017.
- Bouillon, S., Fichet, T., Legat, V., and Madec, G.: The elastic–viscous–plastic method revisited, *Ocean Modelling*, 71, 2–12, <https://doi.org/10.1016/j.ocemod.2013.05.013>, 2013.
- 20 Boutin, G., Ardhuin, F., Dumont, D., Sévigny, C., Girard-Ardhuin, F., and Accensi, M.: Floe Size Effect on Wave-Ice Interactions: Possible Effects, Implementation in Wave Model, and Evaluation, *Journal of Geophysical Research: Oceans*, 123, 4779–4805, <https://doi.org/10.1029/2017JC013622>, 2018.
- Brodeau, L., Barnier, B., Treguier, A.-M., Penduff, T., and Gulev, S.: An ERA40-based atmospheric forcing for global ocean circulation models, *Ocean Modelling*, 31, 88–104, 2010.
- Cheng, S., Rogers, W. E., Thomson, J., Smith, M., Doble, M. J., Wadhams, P., Kohout, A. L., Lund, B., Persson, O. P., Collins, C. O., et al.: Calibrating a viscoelastic sea ice model for wave propagation in the arctic fall marginal ice zone, *Journal of Geophysical Research: Oceans*, 122, 8770–8793, 2017.
- Chevallier, M., Smith, G. C., Dupont, F., Lemieux, J.-F., Forget, G., Fujii, Y., Hernandez, F., Msadek, R., Peterson, K. A., Storto, A., et al.: Intercomparison of the Arctic sea ice cover in global ocean–sea ice reanalyses from the ORA-IP project, *Climate Dynamics*, 49, 1107–1136, 2017.
- 30

- Collins, III, C. O., Rogers, W. E., Marchenko, A., and Babanin, A. V.: In situ measurements of an energetic wave event in the Arctic marginal ice zone, *Geophys. Res. Lett.*, 42, 1863–1870, <https://doi.org/10.1002/2015GL063063>, 2015.
- Comiso, J. C., Meier, W. N., and Gersten, R.: Variability and trends in the Arctic Sea ice cover: Results from different techniques, *Journal of Geophysical Research: Oceans*, 2017.
- Couvelard, X., Lemarié, F., Samson, G., Redelsperger, J.-L., Arduin, F., Benshila, R., and Madec, G.: Development of a 2-way coupled ocean-wave model: assessment on a global oceanic configuration, *Geoscientific Model Development*, Submitted.
- Craig, A., Valcke, S., and Coquart, L.: Development and performance of a new version of the OASIS coupler, *OASIS3-MCT_3. 0*, *Geoscientific Model Development*, 10, 3297, 2017.
- Day, J. J. and Hodges, K. I.: Growing land-sea temperature contrast and the intensification of Arctic cyclones, *Geophysical Research Letters*, 45, 3673–3681, 2018.
- Day, J. J., Holland, M. M., and Hodges, K. I.: Seasonal differences in the response of Arctic cyclones to climate change in CESM1, *Climate dynamics*, 50, 3885–3903, 2018.
- Dumont, D., Kohout, A., and Bertino, L.: A wave-based model for the marginal ice zone including a floe breaking parameterization, *J. Geophys. Res.*, 116, C00E03, <https://doi.org/10.1029/2010JC006682>, 2011.
- Dupont, F., Higginson, S., Bourdallé-Badie, R., Lu, Y., Roy, F., Smith, G., Lemieux, J., Garric, G., and Davidson, F.: A high-resolution ocean and sea-ice modelling system for the Arctic and North Atlantic oceans, *Geoscientific Model Development*, 8, 1577, 2015.
- Feltham, D. L.: Granular flow in the marginal ice zone, *Philosophical Transactions of the Royal Society of London A: Mathematical, Physical and Engineering Sciences*, 363, 1677–1700, 2005.
- Herman, A., Evers, K.-U., and Reimer, N.: Floe-size distributions in laboratory ice broken by waves, *The Cryosphere*, 12, 685–699, 2018.
- Hibler III, W. D.: A Dynamic Thermodynamic Sea Ice Model, *Journal of Physical Oceanography*, 9, 815–846, [https://doi.org/10.1175/1520-0485\(1979\)009<0815:ADTSIM>2.0.CO;2](https://doi.org/10.1175/1520-0485(1979)009<0815:ADTSIM>2.0.CO;2), 1979.
- Horvat, C. and Tziperman, E.: A prognostic model of the sea-ice floe size and thickness distribution, *The Cryosphere*, 9, 2119–2134, <https://doi.org/10.5194/tc-9-2119-2015>, <http://www.the-cryosphere.net/9/2119/2015/>, 2015.
- Hunke, E. C. and Dukowicz, J. K.: An Elastic–Viscous–Plastic Model for Sea Ice Dynamics, *Journal of Physical Oceanography*, 27, 1849–1867, [https://doi.org/10.1175/1520-0485\(1997\)027<1849:AEVPMF>2.0.CO;2](https://doi.org/10.1175/1520-0485(1997)027<1849:AEVPMF>2.0.CO;2), 1997.
- Inoue, J., Wakatsuchi, M., and Fujiyoshi, Y.: Ice floe distribution in the Sea of Okhotsk in the period when sea-ice extent is advancing, *Geophysical research letters*, 31, 2004.
- Jackson, J., Carmack, E., McLaughlin, F., Allen, S. E., and Ingram, R.: Identification, characterization, and change of the near-surface temperature maximum in the Canada Basin, 1993–2008, *Journal of Geophysical Research: Oceans*, 115, 2010.
- Khon, V., Mokhov, I., Pogarskiy, F., Babanin, A., Dethloff, K., Rinke, A., and Matthes, H.: Wave heights in the 21st century Arctic Ocean simulated with a regional climate model, *Geophysical Research Letters*, 41, 2956–2961, 2014.
- Kohout, A. L., Williams, M. J. M., Dean, S. M., and Meylan, M. H.: Storm-induced sea-ice breakup and the implications for ice extent, *Nature*, 509, 604–607, <https://doi.org/10.1038/nature13262>, 2014.
- Langhorne, P. J., Squire, V. A., Fox, C., and Haskell, T. G.: Break-up of sea ice by ocean waves, *Annals of Glaciology*, 27, 438–442, 1998.
- Lee, C. M., Cole, S., Doble, M., Freitag, L., Hwang, P., Jayne, S., Jeffries, M., Krishfield, R., Maksym, T., and Maslowski, W.: Marginal Ice Zone (MIZ) program: Science and experiment plan, Tech. rep., WASHINGTON UNIV SEATTLE APPLIED PHYSICS LAB, 2012.
- Lemieux, J.-F., Lei, J., Dupont, F., Roy, F., Losch, M., Lique, C., and Laliberté, F.: The Impact of Tides on Simulated Landfast Ice in a Pan-Arctic Ice-Ocean Model, *Journal of Geophysical Research: Oceans*, 123, 7747–7762, 2018.

- Lique, C., Holland, M. M., Dibike, Y. B., Lawrence, D. M., and Screen, J. A.: Modeling the Arctic freshwater system and its integration in the global system: Lessons learned and future challenges, *Journal of Geophysical Research: Biogeosciences*, 121, 540–566, 2016.
- Longuet-Higgins, M. S.: The mean forces exerted by waves on floating or submerged bodies with applications to sand bars and wave power machines, *Proc. Roy. Soc. Lond. A*, 352, 463–480, 1977.
- Longuet-Higgins, M. S. and Stewart, R. W.: Radiation stresses and mass transport in surface gravity waves with application to ‘surf beats’, *J. Fluid Mech.*, 13, 481–504, 1962.
- Lüpkes, C., Gryanik, V. M., Hartmann, J., and Andreas, E. L.: A parametrization, based on sea ice morphology, of the neutral atmospheric drag coefficients for weather prediction and climate models, *Journal of Geophysical Research: Atmospheres*, 117, 2012.
- Madec, G.: NEMO ocean engine, Note du Pôle de modélisation, Institut Pierre-Simon Laplace (IPSL), France, No 27, ISSN No 1288-1619, 2008.
- Marcq, S. and Weiss, J.: Influence of sea ice lead-width distribution on turbulent heat transfer between the ocean and the atmosphere, *The Cryosphere*, 6, 143–156, 2012.
- Martin, S. and Kauffman, P.: A Field and Laboratory Study of Wave Damping by Grease Ice, *Journal of Glaciology*, 27, 283–313, <https://doi.org/10.1017/S0022143000015392>, 1981.
- Maykut, G. A. and Perovich, D. K.: The role of shortwave radiation in the summer decay of a sea ice cover, *Journal of Geophysical Research: Oceans*, 92, 7032–7044, 1987.
- McPhee, M. G.: An analysis of pack ice drift in summer, *Sea ice processes and models*, pp. 62–75, 1980.
- Mellor, M.: Mechanical Behavior of Sea Ice, in: *The Geophysics of Sea Ice*, edited by Untersteiner, N., NATO ASI Series, pp. 165–281, Springer US, https://doi.org/10.1007/978-1-4899-5352-0_3, 1986.
- Montiel, F., Squire, V. A., and Bennetts, L. G.: Attenuation and directional spreading of ocean wave spectra in the marginal ice zone, *J. Fluid Mech.*, 790, 492–522, <https://doi.org/10.1017/jfm.2016.2>, 2016.
- Perrie, W. and Hu, Y.: Air–ice–ocean momentum exchange. Part II: Ice drift, *Journal of physical oceanography*, 27, 1976–1996, 1997.
- Rainville, L., Lee, C. M., and Woodgate, R. A.: Impact of wind-driven mixing in the Arctic Ocean, *Oceanography*, 24, 136–145, 2011.
- Rampal, P., Bouillon, S., Olason, E., and Morlighem, M.: neXtSIM: a new Lagrangian sea ice model, *CRYOSPHERE*, 10, <https://doi.org/10.5194/tc-10-1055-2016>, 2016.
- Roach, L. A., Horvat, C., Dean, S. M., and Bitz, C. M.: An emergent sea ice floe size distribution in a global coupled ocean–sea ice model, *Journal of Geophysical Research: Oceans*, 2018.
- Rogers, W. E., Thomson, J., Shen, H. H., Doble, M. J., Wadhams, P., and Cheng, S.: Dissipation of wind waves by pancake and frazil ice in the autumn Beaufort Sea, *J. Geophys. Res.*, 121, <https://doi.org/10.1002/2016JC012251>, 2016.
- Rothrock, D. and Thorndike, A.: Measuring the sea ice floe size distribution, *Journal of Geophysical Research: Oceans*, 89, 6477–6486, 1984.
- Rousset, C., Vancoppenolle, M., Madec, G., Fichet, T., Flavoni, S., Barthélemy, A., Benshila, R., Chanut, J., Lévy, C., Masson, S., et al.: The Louvain-La-Neuve sea ice model LIM3. 6: global and regional capabilities, *Geoscientific Model Development*, 8, 2991, 2015.
- Shen, H. H. and Ackley, S. F.: A one-dimensional model for wave-induced ice-floe collisions, *Annals of Glaciology*, 15, 87–95, 1991.
- Smith, M., Stammerjohn, S., Persson, O., Rainville, L., Liu, G., Perrie, W., Robertson, R., Jackson, J., and Thomson, J.: Episodic reversal of autumn ice advance caused by release of ocean heat in the Beaufort Sea, *Journal of Geophysical Research: Oceans*, 2018.
- Squire, V. A.: A fresh look at how ocean waves and sea ice interact, *Phil. Trans. R. Soc. A*, 376, 20170342, 2018.
- Steele, K., Teng, C.-C., and Wang, D. W.-C.: Wave direction measurements using pitch and roll buoys, *Ocean Eng.*, 19, 349–375, 1992.

- Steele, M.: Sea ice melting and floe geometry in a simple ice-ocean model, *Journal of Geophysical Research: Oceans*, 97, 17 729–17 738, <https://doi.org/10.1029/92JC01755>, 1992.
- Steele, M., Morison, J. H., and Untersteiner, N.: The partition of air-ice-ocean momentum exchange as a function of ice concentration, floe size, and draft, *Journal of Geophysical Research: Oceans*, 94, 12 739–12 750, 1989.
- Stopa, J., Ardhuin, F., Thomson, J., Smith, M. M., Kohout, A., Doble, M., and Wadhams, P.: Wave Attenuation Through an Arctic Marginal Ice Zone on 12 October, 2015: 1. Measurement of Wave Spectra and Ice Features From Sentinel-1A, *Journal of Geophysical Research: Oceans*, 2018a.
- Stopa, J. E., Ardhuin, F., and Girard-Ardhuin, F.: Wave climate in the Arctic 1992-2014: seasonality and trends, *The Cryosphere*, 10, 1605–1629, <https://doi.org/10.5194/tc-10-1605-2016>, 2016a.
- Stopa, J. E., Ardhuin, F., Husson, R., Jiang, H., Chapron, B., and Collard, F.: Swell dissipation from 10 years of Envisat ASAR in wave mode, *Geophys. Res. Lett.*, 43, 3423–3430, <https://doi.org/10.1002/2015GL067566>, 2016b.
- Stopa, J. E., Sutherland, P., and Ardhuin, F.: Strong and highly variable push of ocean waves on Southern Ocean sea ice, *Proceedings of the National Academy of Sciences*, 115, 5861–5865, 2018b.
- Stroeve, J., Hamilton, L. C., Bitz, C. M., and Blanchard-Wrigglesworth, E.: Predicting September sea ice: Ensemble skill of the SEARCH Sea Ice Outlook 2008-2013, *Geophys. Res. Lett.*, 41, 2411–2418, <https://doi.org/10.1002/2014GL059388>, 2014.
- Strong, C. and Rigor, I. G.: Arctic marginal ice zone trending wider in summer and narrower in winter, *Geophysical Research Letters*, 40, 4864–4868, <https://doi.org/10.1002/grl.50928>, 2013.
- Sutherland, P. and Dumont, D.: Marginal ice zone thickness and extent due to wave radiation stress., *Journal of Physical Oceanography*, 2018.
- Sutherland, P. and Melville, W. K.: Field measurements and scaling of ocean surface wave-breaking statistics, *Geophys. Res. Lett.*, 40, 3074–3079, <https://doi.org/10.1002/grl.50584>, 2013.
- The WAVEWATCH III® Development Group: User manual and system documentation of WAVEWATCH III® version 5.16, Tech. Note 329, NOAA/NWS/NCEP/MMAB, College Park, MD, USA, 326 pp. + Appendices, 2016.
- Thomson, J. and Rogers, W. E.: Swell and sea in the emerging Arctic Ocean, *Geophys. Res. Lett.*, 41, 3136–3140, <https://doi.org/10.1002/2014GL059983>, 2014.
- Thomson, J., Ackley, S., Girard-Ardhuin, F., Ardhuin, F., Babanin, A., Bidlot, J., Boutin, G., Brozena, J., Cheng, S., Doble, M., et al.: Overview of the arctic sea state and boundary layer physics program, *Journal of Geophysical Research: Oceans*, 2018.
- Timmermans, M.-L.: The impact of stored solar heat on Arctic sea ice growth, *Geophysical Research Letters*, 42, 6399–6406, 2015.
- Toyota, T., Haas, C., and Tamura, T.: Size distribution and shape properties of relatively small sea-ice floes in the Antarctic marginal ice zone in late winter, *Deep Sea Research Part II: Topical Studies in Oceanography*, 58, 1182–1193, 2011.
- Uotila, P., Goosse, H., Haines, K., Chevallier, M., Barthélemy, A., Bricaud, C., Carton, J., Fučkar, N., Garric, G., Iovino, D., et al.: An assessment of ten ocean reanalyses in the polar regions, *Climate Dynamics*, pp. 1–38, 2018.
- Vancoppenolle, M., Fichefet, T., Goosse, H., Bouillon, S., Madec, G., and Maqueda, M. A. M.: Simulating the mass balance and salinity of Arctic and Antarctic sea ice. 1. Model description and validation, *Ocean Modelling*, 27, 33–53, 2009.
- Wang, Q., Ilicak, M., Gerdes, R., Drange, H., Aksenov, Y., Bailey, D. A., Bentsen, M., Biastoch, A., Bozec, A., Böning, C., et al.: An assessment of the Arctic Ocean in a suite of interannual CORE-II simulations. Part II: Liquid freshwater, *Ocean Modelling*, 99, 86–109, 2016.

- Waseda, T., Webb, A., Sato, K., Inoue, J., Kohout, A., Penrose, B., and Penrose, S.: Correlated Increase of High Ocean Waves and Winds
 930 in the Ice-Free Waters of the Arctic Ocean, *Scientific Reports*, 8, 4489, <https://doi.org/10.1038/s41598-018-22500-9>, <https://doi.org/10.1038/s41598-018-22500-9>, 2018.
- Williams, T. D., Bennetts, L. G., Squire, V. A., Dumont, D., and Bertino, L.: Wave-ice interactions in the marginal ice zone. Part 2: Numerical implementation and sensitivity studies along 1D transects of the ocean surface, *Ocean Modelling*, 71, 92–101, <https://doi.org/10.1016/j.ocemod.2013.05.011>, 2013.
- 935 Williams, T. D., Rampal, P., and Bouillon, S.: Wave-ice interactions in the neXtSIM sea-ice model, *The Cryosphere Discussions*, pp. 1–28, <https://doi.org/10.5194/tc-2017-24>, 2017.
- Zhang, J., Schweiger, A., Steele, M., and Stern, H.: Sea ice floe size distribution in the marginal ice zone: Theory and numerical experiments: Modeling floe size distribution, *Journal of Geophysical Research: Oceans*, 120, 3484–3498, <https://doi.org/10.1002/2015JC010770>, 2015.
- Zhang, J., Stern, H., Hwang, B., Schweiger, A., Steele, M., Stark, M., and Graber, H. C.: Modeling the seasonal evolution of the Arctic sea
 940 ice floe size distribution, *Elementa*, 4, <https://doi.org/10.12952/journal.elementa.000126>, 2016.
- Zhao, J., Barber, D., Zhang, S., Yang, Q., Wang, X., and Xie, H.: Record low sea-ice concentration in the central Arctic during summer 2010, *Advances in Atmospheric Sciences*, 35, 106–115, 2018.

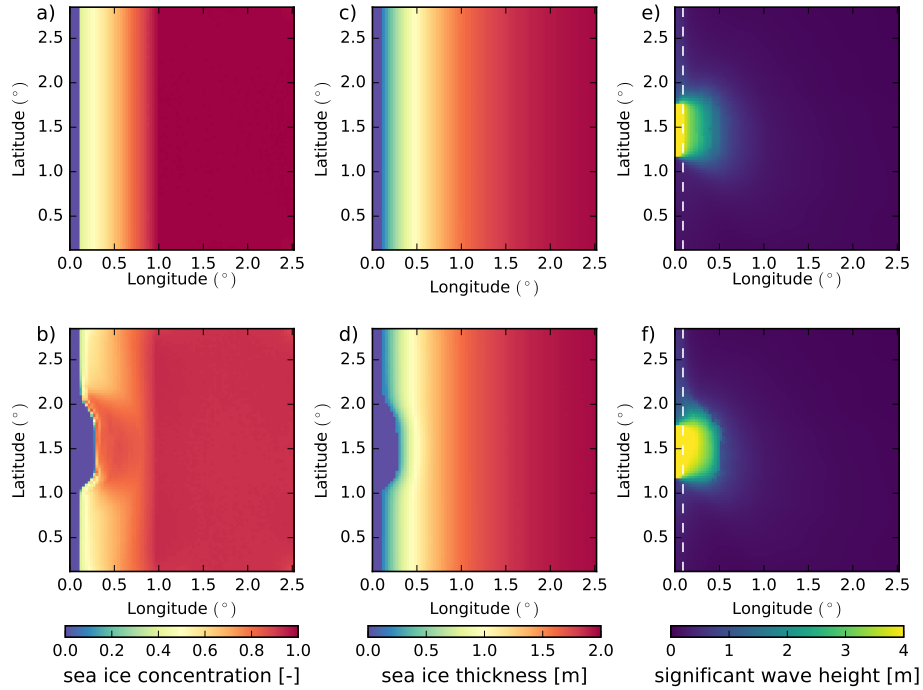


Figure 1. Implementation of the WRS in the idealized configuration. (a) and (c) show the initial state of sea ice concentration and thickness (ice-cover average), respectively. (b) and (d) show sea ice concentration and thickness after 72 h in the WW3-LIM3 coupled model. (e) and (f) show the significant wave height H_s distribution after 72 h in the WW3 model and in the WW3-LIM3 coupled model, respectively. The white dashed line on (e) and (f) indicates the position of the ice edge ($c=0.15$).

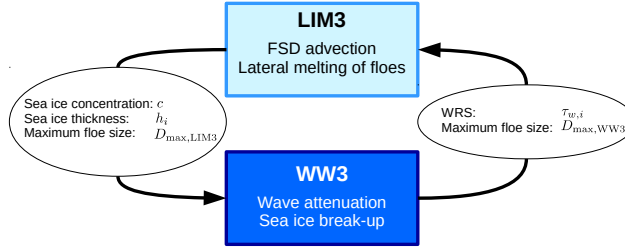


Figure 2. Schematic ~~summarizing-summary~~ of the exchanged information between the sea ice model LIM3 and the wave model WAVE-WATCH III® in our coupled framework. The two boxes ~~corresponds~~ correspond to the processes accounted for in a given model, while the variables exchanged between the models are listed in the bubbles.

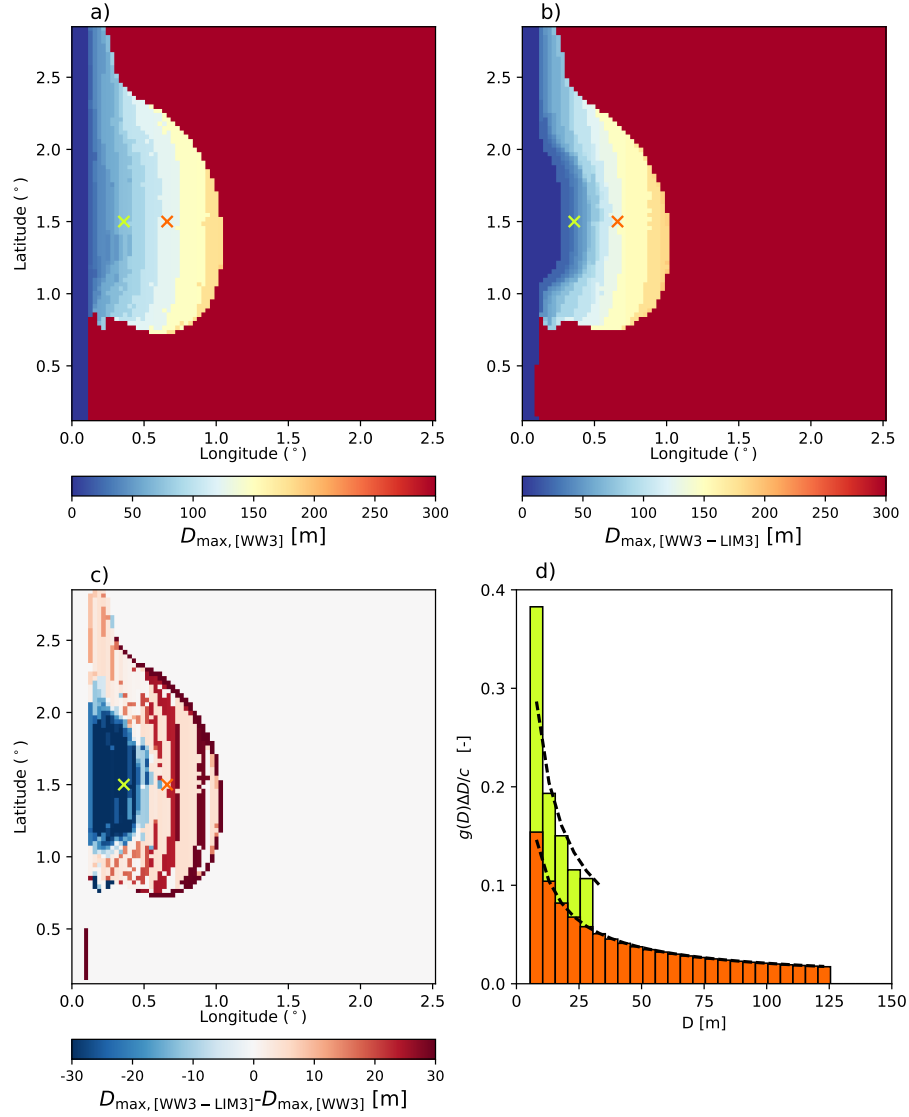


Figure 3. Snapshots of D_{\max} from the uncoupled WW3 (a) and the WW3-LIM3 (b) simulations after 72 h, and the difference between the two (c). Panel (d) shows the FSD from the WW3-LIM3 run at two locations indicated with crosses on panels a,b,c. The black dashed line in (d) corresponds to the theoretical power-law FSD assumed in WW3.

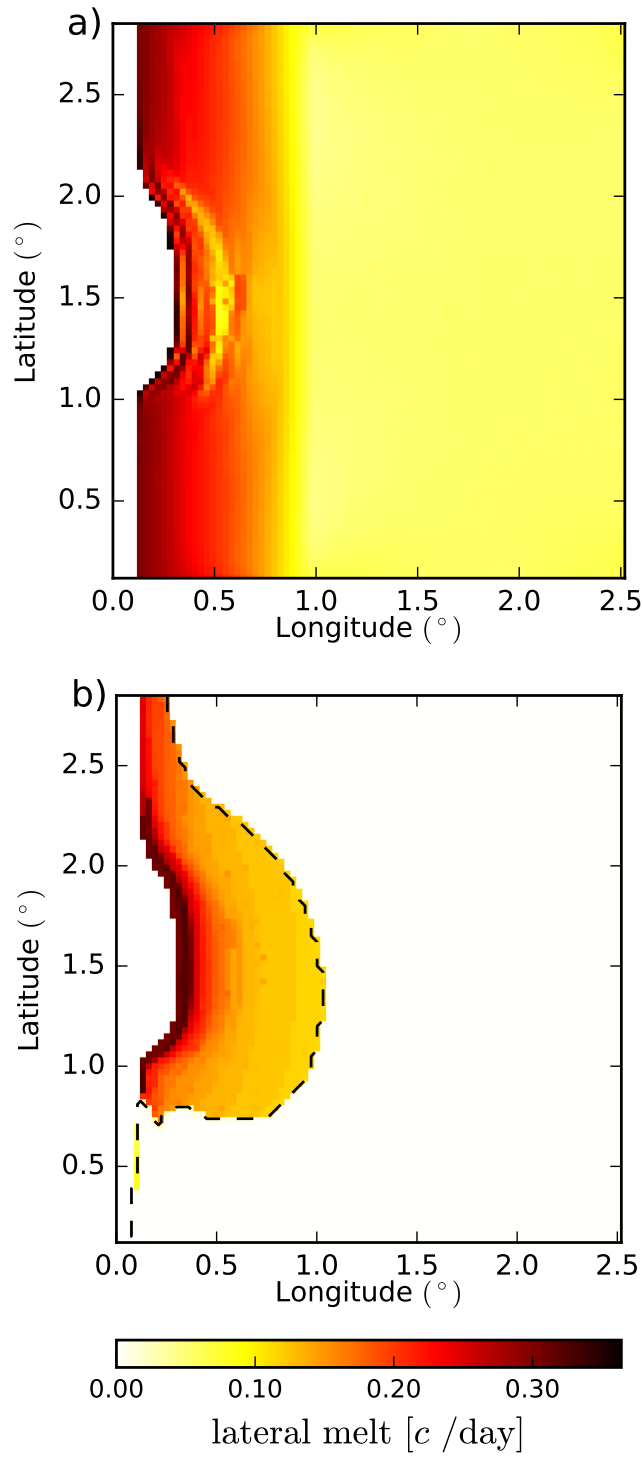


Figure 4. Lateral melt rates [estimated as percentage of sea ice concentration lost per day] estimated by the coupled model after 72 h of simulation using the parameterization of Lüpkes et al. (2012) (a), or the parameterization developed in this study accounting for wave-induced sea ice break-up fragmentation (b). The black dashed contour on panel (b) indicates $D_{\max} = 500 m$, and thus represents the limit between broken and unbroken sea ice.

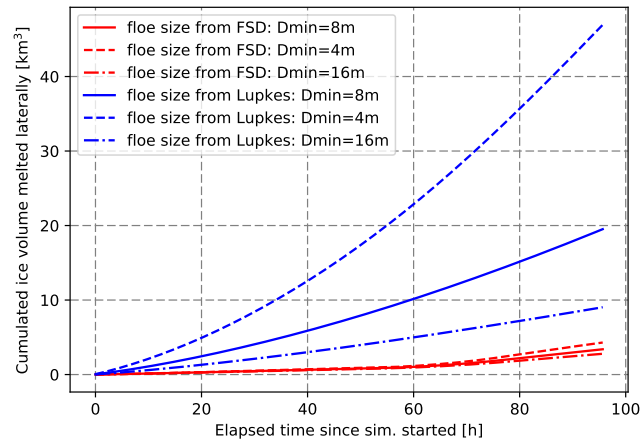


Figure 5. Temporal evolution of the sea ice volume loss due to lateral melt integrated over the whole domain for simulations similar to the one presented in Fig. 4, but for different values of D_{\min} . The two colors correspond to the two lateral melt parameterizations used in this study.

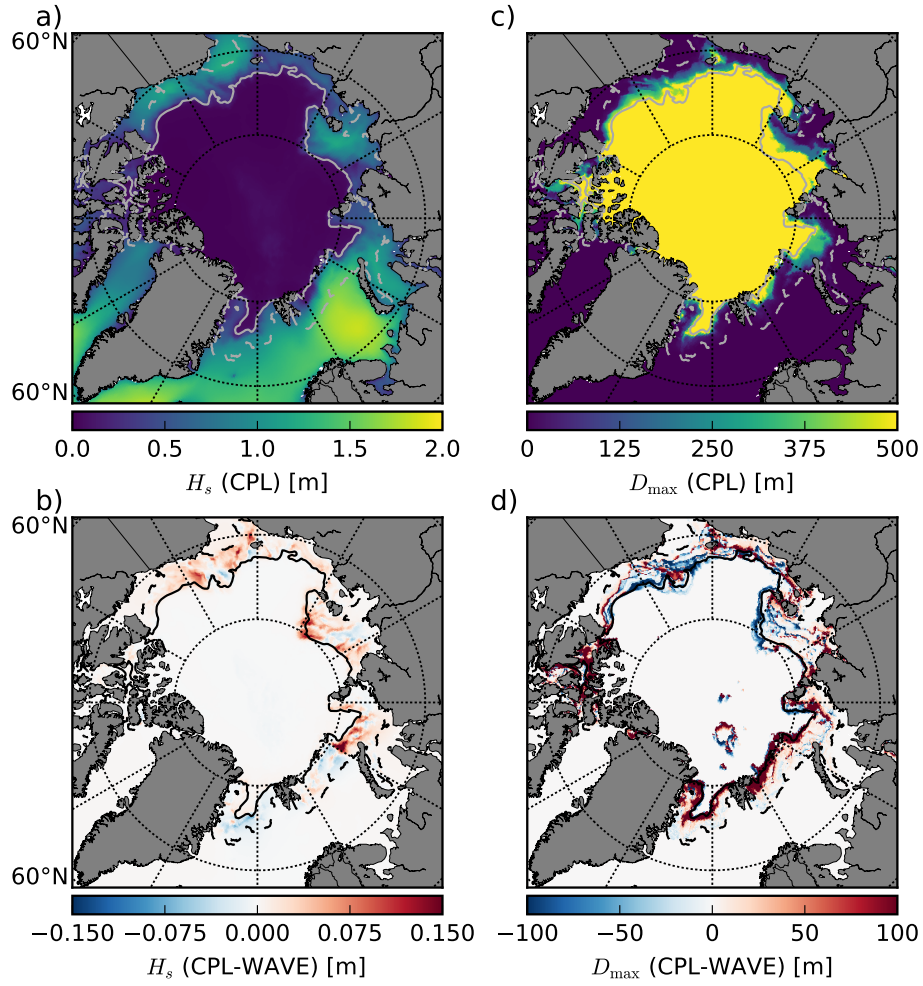


Figure 6. Significant wave height (a) and maximum floe size (c) in the CPL simulation averaged over the period 03-08-2010 to 09-09-2018, and the differences with the WAVE simulations (b, d). The black and grey contours delimit the MIZ in the CPL simulation, defined here as $0 < \langle D_{\max} \rangle < 700$ m. Note that the sea ice conditions from the NOT_CPL run are used as forcing for the WAVE run and are thus similar in the WAVE and the NOT_CPL runs.

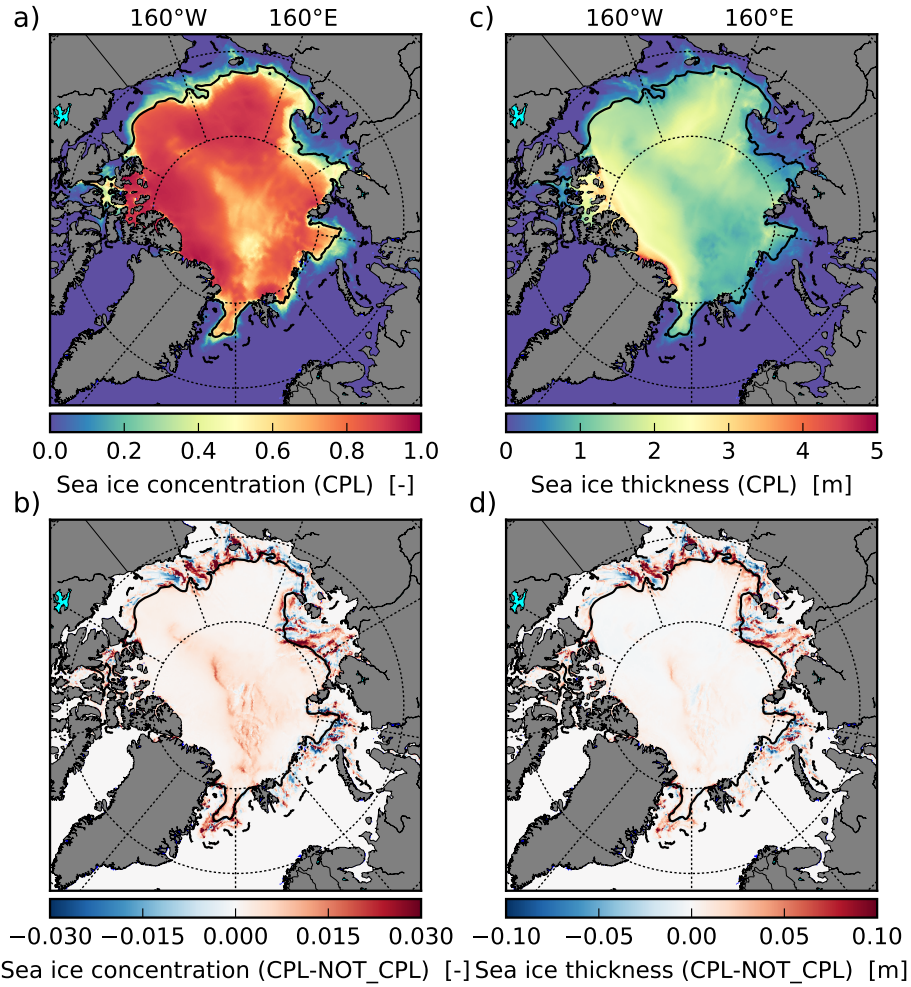


Figure 7. Sea ice concentration and thickness in the CPL simulation (a, c) and the difference with NOT_CPL (b,d) averaged over the period 04/08/2010 to 09/09/2010. The black contours delimit the MIZ in the CPL simulation, defined here as $0 < \langle D_{\max} \rangle < 700$ m.

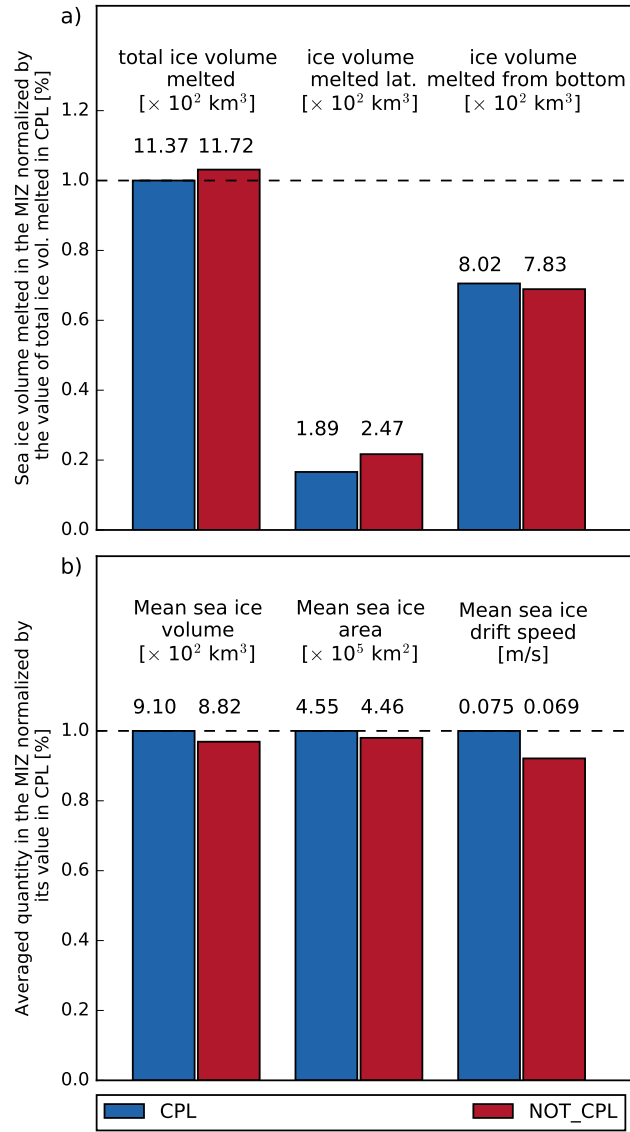


Figure 8. (a) Sea ice volume melted (in 10^2 km^3) integrated over the MIZ and over the period between 04/08/2010 and 09/09/2010 in the CPL and the NOT_CPL simulations. Here the MIZ is defined as the region where $0 < \langle D_{\max} \rangle < 700$ m in the CPL run. The contribution from lateral melt and bottom melt to the total melt for both simulations are also represented. (b) Mean sea ice volume (in 10^2 km^3), area (in 10^5 km^2), and drift speed (in m/s) in the MIZ over the same period. Values for each simulation are found above their associated bar.

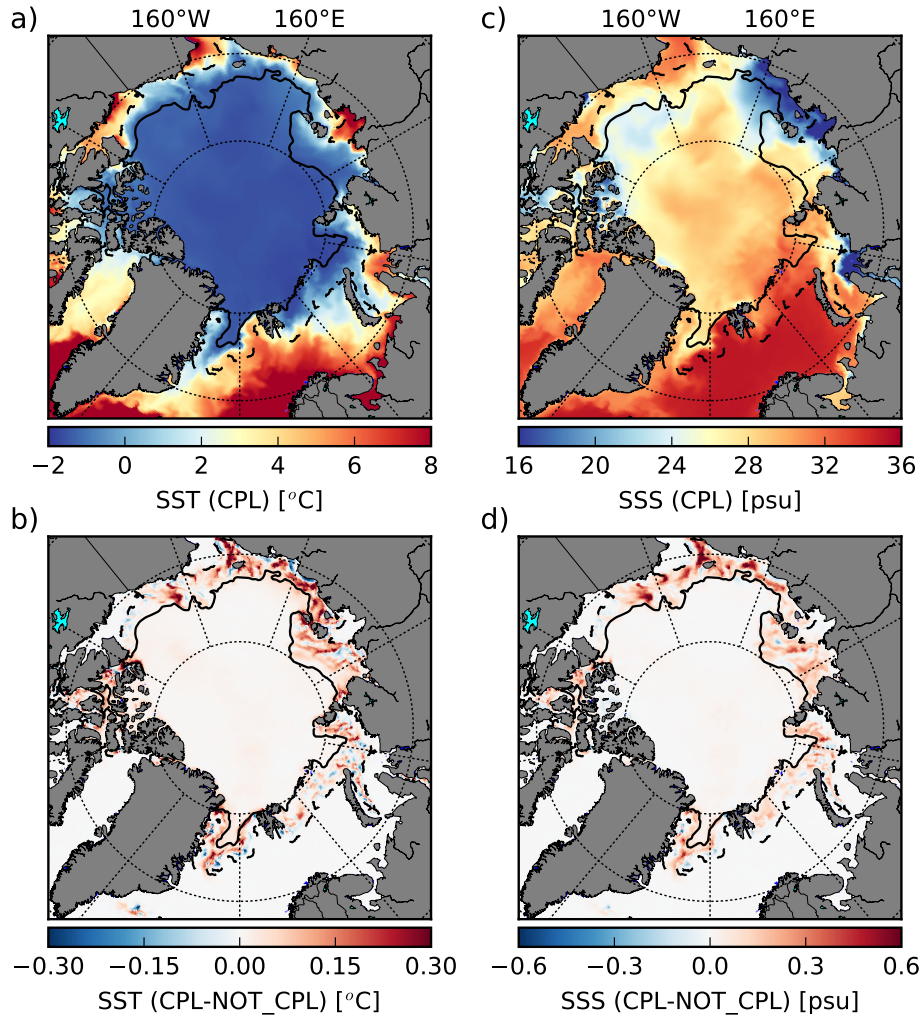


Figure 9. SST (a) and SSS (c) in the CPL run for the period between between 04/08/2010 and 09/09/2010, and the difference with NOT_CPL (b,d). The black contours delimit the MIZ in the CPL simulation, defined here as $0 < \langle D_{\max} \rangle < 700$ m.

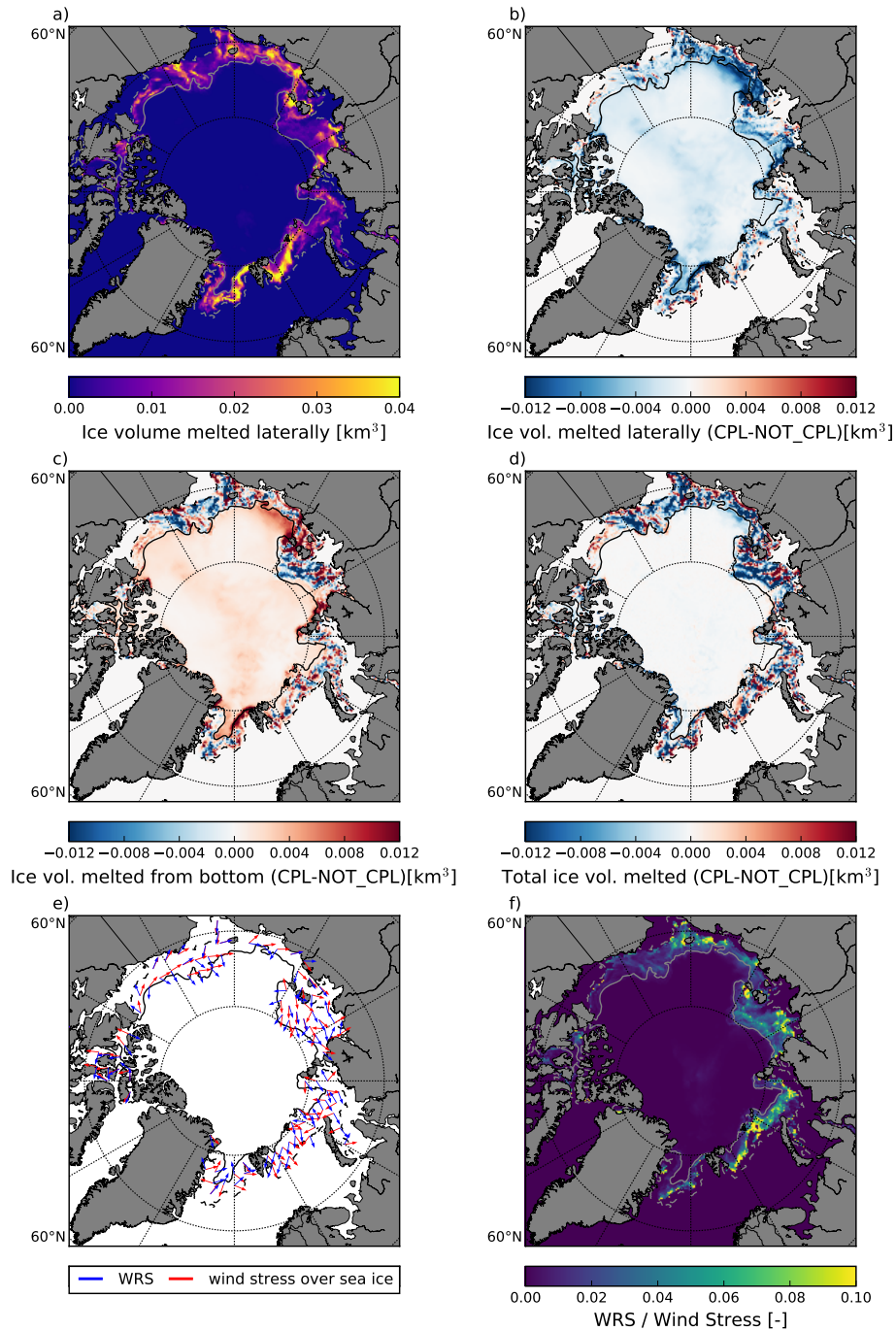


Figure 10. Volume of sea ice melted by lateral melt in the CPL simulation over the period between 04/08/2010 and 09/09/2010 (a). Differences between the CPL and the NOT_CPL runs of lateral melt (b), bottom melt (c) and total melt (d). (e) Wind stress (red) and WRS (blue) averaged over the same period 04/08/2010 and 09/09/2010 in the CPL simulation. Note that the WRS has been multiplied by a factor of 10 in order to improve readability. (f) Distribution of the relative magnitude of WRS over the wind stress. The grey contours represent the position of the ice edge ($c = 0.15$) on the first (solid line) and last day (dashed line) of the period considered in the CPL simulation.

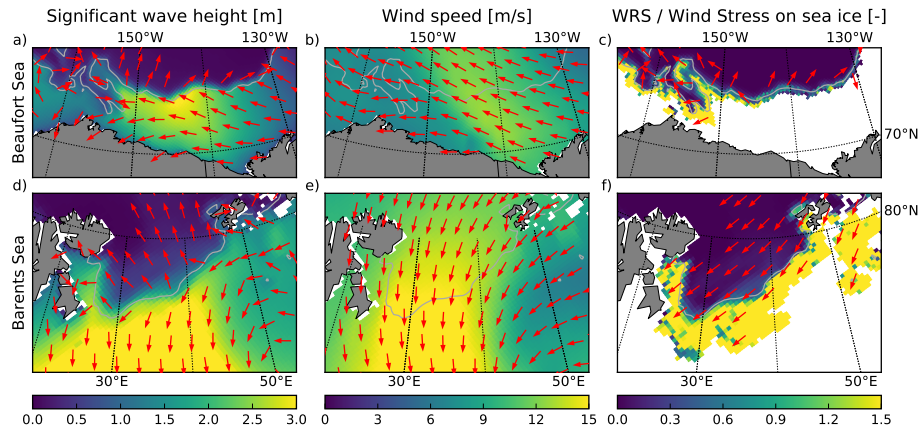


Figure 11. Significant wave height and wave mean direction of propagation (a, d), wind speed (b, e) and WRS (c, f) simulated by the CPL run during the storms that occurred in the Beaufort Sea (a, b, c) and in the Barents Sea (d, e, f) on 16/08/2010-17/08/2010. The grey contours indicate the position of the sea ice edge determined from the averaged sea ice concentration ($c = 0.15$).

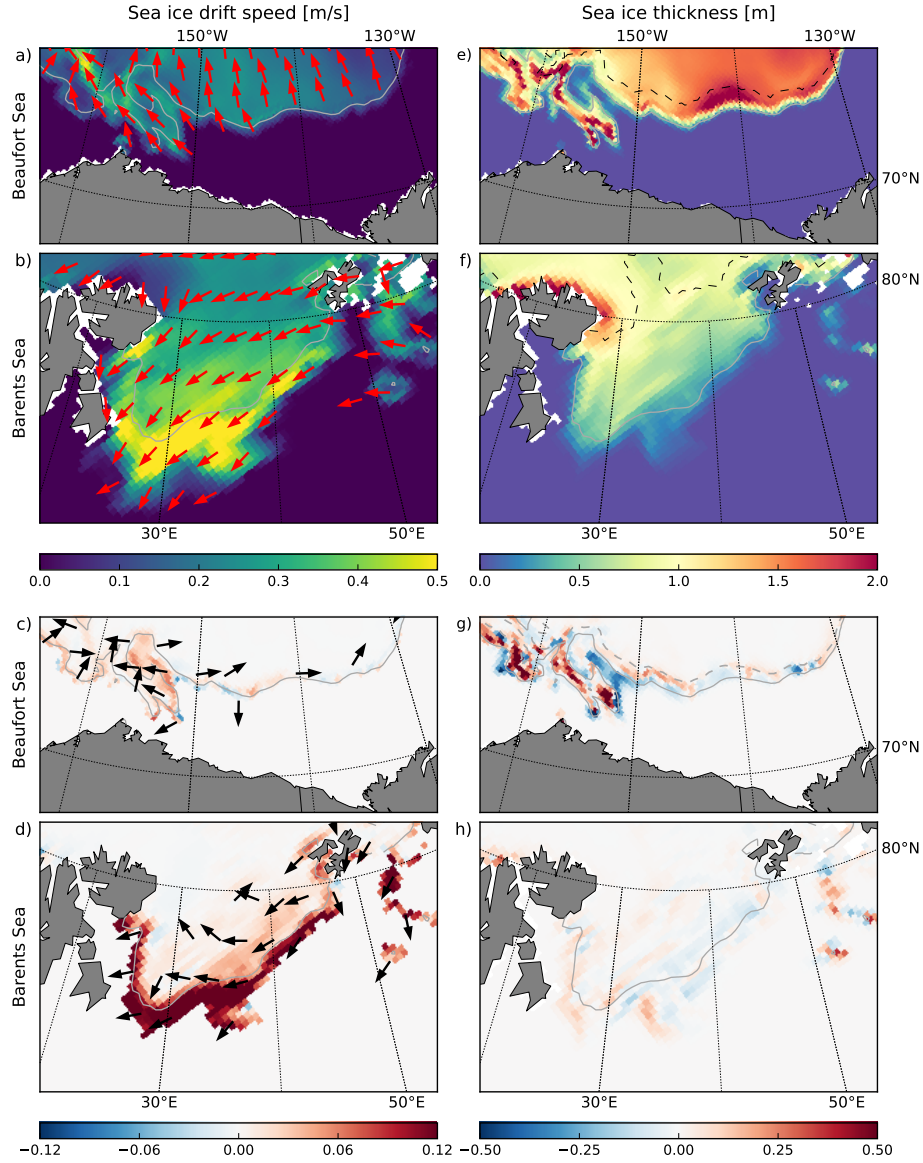


Figure 12. Mean sea ice drift (a, b) and sea ice thickness (e, f) simulated by the CPL run during the storms that occurred in the Beaufort Sea (a, c) and in the Barents Sea (b, f) on 16/08/2010-17/08/2010. Panels (c, d, g, h) show the differences for these quantities between the CPL and NOT_CPL simulations. Grey contours indicate the position of the ice edge determined from the averaged sea ice concentration ($c = 0.15$). The black dashed contour delimits the border between broken and unbroken ice ($D_{\max} = 500\text{m}$)

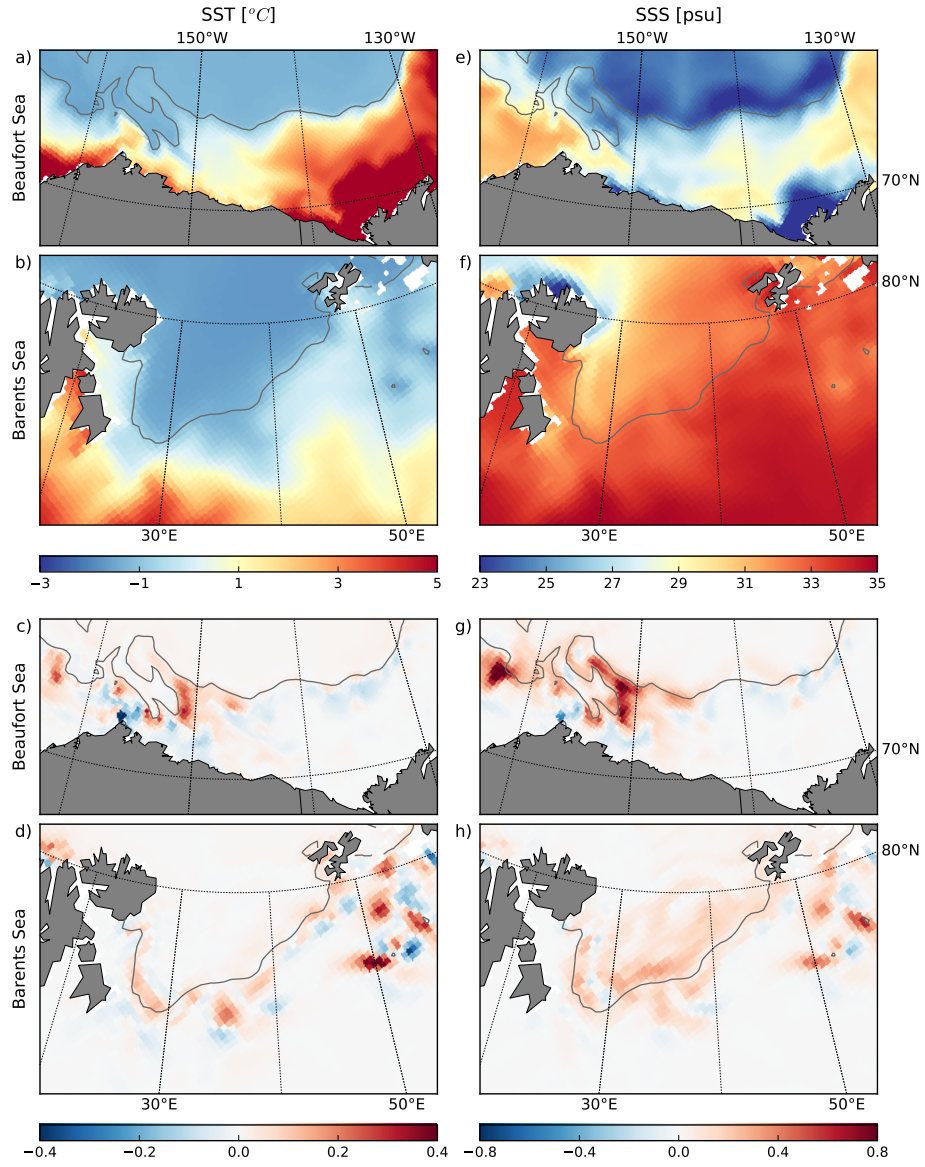


Figure 13. SST (a, b) and SSS (e, f) simulated by the CPL run during the storms that occurred in the Beaufort Sea (a, c) and in the Barents Sea (b, f) on 16/08/2010-17/08/2010. Panels (c, d, g, h) show the differences for these quantities between the CPL and NOT_CPL simulations. Grey contours indicate the position of the ice edge determined from the averaged sea ice concentration ($c = 0.15$).

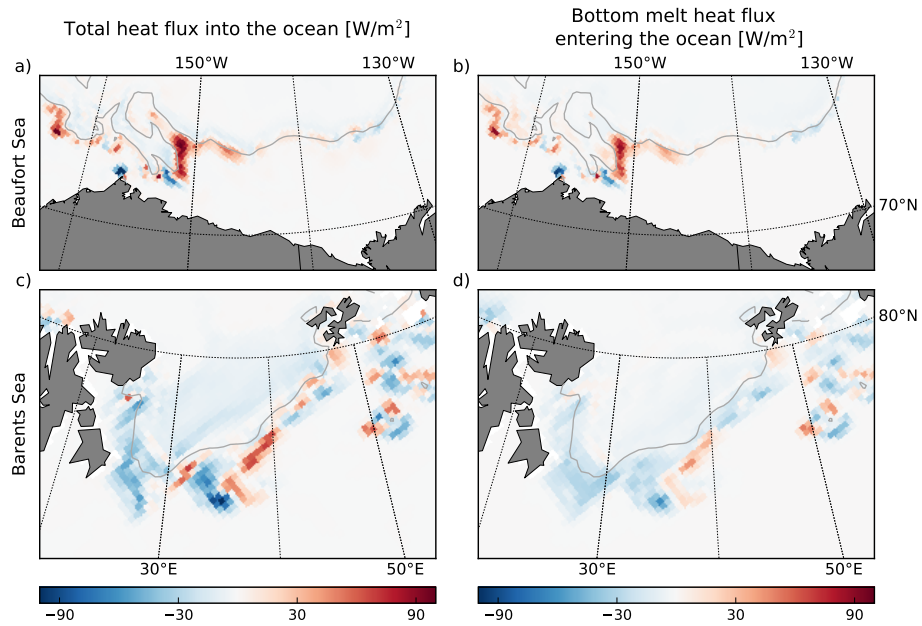


Figure 14. Averaged differences between the CPL and NOT_CPL simulations of (a, c) the heat flux into the ocean and (b, d) the contribution to the heat flux into the ocean coming from the sea ice bottom melt during the storms in the Beaufort Sea (a, b) and in the Barents Sea (c, d) which occurred on 16/08/2010-17/08/2010. Grey contours indicate the position of the ice edge determined from the averaged sea ice concentration ($c = 0.15$).